

# Universal non-Hermitian skin effect in two and higher dimensions

Kai Zhang,<sup>1,2</sup> Zhesen Yang,<sup>3,\*</sup> and Chen Fang<sup>1,3,4,†</sup>

<sup>1</sup>*Beijing National Laboratory for Condensed Matter Physics and Institute of Physics,  
Chinese Academy of Sciences, Beijing 100190, China*

<sup>2</sup>*University of Chinese Academy of Sciences, Beijing 100049, China*

<sup>3</sup>*Kavli Institute for Theoretical Sciences, Chinese Academy of Sciences, Beijing 100190, China*

<sup>4</sup>*Songshan Lake Materials Laboratory, Dongguan, Guangdong 523808, China*

Skin effect, experimentally discovered in one dimension, describes the physical phenomenon that on an open chain, an extensive number of eigenstates of a non-Hermitian hamiltonian are localized at the end(s) of the chain. Here in two and higher dimensions, we establish a theorem that the skin effect exists, if and only if periodic-boundary spectrum of the hamiltonian covers a finite area on the complex plane. This theorem establishes the universality of the effect, because the above condition is satisfied in almost every generic non-Hermitian hamiltonian, and, unlike in one dimension, is compatible with all spatial symmetries. We propose two new types of skin effect in two and higher dimensions: the corner-skin effect where all eigenstates are localized at one corner of the system, and the geometry-dependent-skin effect where skin modes disappear for systems of a particular shape, but appear on generic polygons. An immediate corollary of our theorem is that any non-Hermitian system having exceptional points (lines) in two (three) dimensions exhibits skin effect, making this phenomenon accessible to experiments in photonic crystals, Weyl semimetals, and Kondo insulators.

## INTRODUCTION

The study of non-Hermitian hamiltonians, which can be regarded as the effective description of dissipative processes, can be traced back to the investigation of alpha decay, where real and imaginary parts of the complex energy are related to the experimentally observed energy level and decay rate [1]. When a lattice system is coupled with environments and has dissipations, e.g. photonic crystals having radiational loss [2–4] and electronic systems having finite quasiparticle lifetime [5–8], the non-Hermitian band theory becomes a conceptually simple and efficient approach [9–16].

Skin effect [17–31], a phenomenon unique to the non-Hermitian band theory, refers to the localization of eigenstates at the boundary, the number of which scales with the volume of the system. For example, in one dimension, all eigenstates of a non-Hermitian hamiltonian can be localized at the ends of a chain [17]. This suggests the failure of Bloch’s theorem [32, 33], which states that eigenstates in the bulk are modulated plane waves. As Bloch’s theorem plays a fundamental role in the development of condensed-matter physics [34], the emergence of skin effect indicates a new and possibly revolutionary direction. Especially, the skin effect has been experimentally observed in one-dimensional classical systems [35–41], inspiring further studies on their higher dimensional generalizations [18, 42–59]. However, a general theory for the higher-dimensional skin effect has not been established.

Apart from the skin effect, another focus topic in non-Hermitian band systems is the exceptional point (or

line) [60–79] that refers to stable point-type (or line-type) non-Hermitian band degeneracy in the Brillouin zone. At the exceptional point, not only eigenvalues but also eigenstates of the Bloch hamiltonian coalesce [61]. Many a novel phenomenon related to exceptional points has been predicted and observed [77, 80–91], such as the emergence of bulk-Fermi arc terminated at the exceptional points [5, 73]. Since the bulk-boundary correspondence plays a central role in the development of topological phases [92], it is natural to ask if there exists a non-Hermitian bulk-boundary correspondence in bands having exceptional points, analogous to the surface Fermi arc in the Weyl semimetals in the Hermitian counterpart [93].

In this paper, we establish a theorem that reveals a universal bulk-boundary correspondence in two and higher dimensional non-Hermitian bands, as shown in Fig. 1. The “bulk” refers to the area of the spectrum of the hamiltonian on the complex plane with periodic boundary condition, and “boundary” the presence (absence) of the skin effect for open-boundary system of an arbitrary shape. The theorem states that the skin effect appears if and only if the spectral area is nonzero. This skin effect is “universal” for three reasons: (i) a randomly generated local non-Hermitian hamiltonian has the skin effect with probability one; (ii) the skin effect is, unlike in one dimension, compatible with all spatial symmetries and time-reversal symmetry; and (iii) it does not require any special geometry of the open-boundary system. We also propose two manifestations, restricted to two and higher dimensions, of the universal skin effect, i.e., the corner-skin effect and the geometry-dependent skin effect.

A surprising corollary of our theorem is that all stable exceptional points [11, 68, 70] imply the presence of skin effect. Because exceptional points have been either observed or proposed in meta-materials as well as in condensed matter, this corollary makes skin effect observable

\* yangzs@ucas.ac.cn

† cfang@iphy.ac.cn

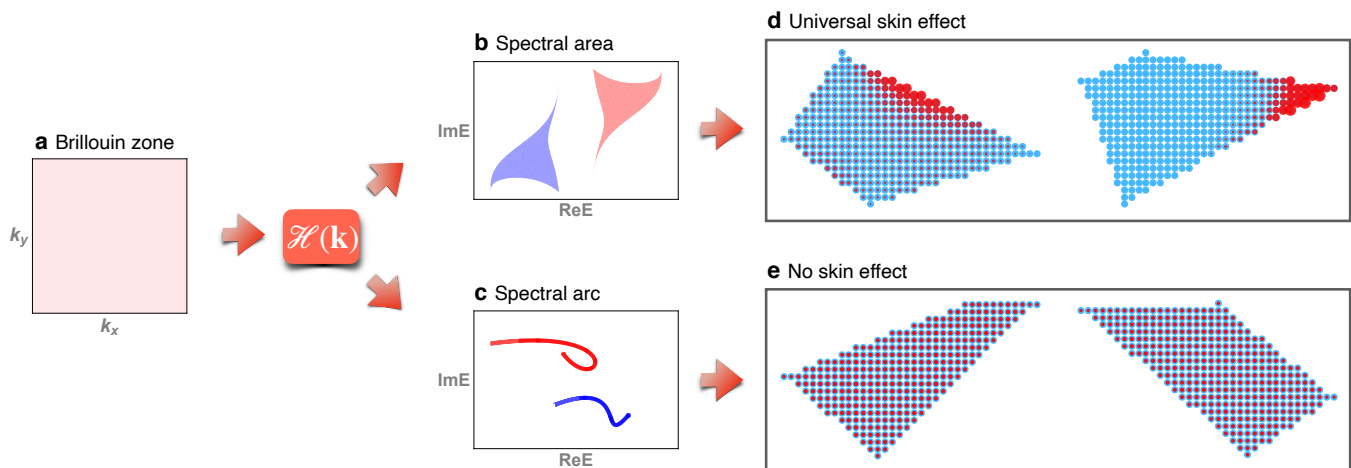


FIG. 1. The theorem of universal skin effect. (a) represents the Brillouin zone. (b)(d) shows that when the spectral area of  $\mathcal{H}(\mathbf{k})$  is nonzero, the system on generic geometries must have universal skin effect. (c)(e) shows that when the spectral area of  $\mathcal{H}(\mathbf{k})$  is zero, or forming one or several arcs on the complex plane, there is no skin effect under any geometry.

in known systems. We predict the geometry-dependent skin effect in the two-dimensional photonic crystal studied in Ref. [73], and propose to observe this effect in the anomalous dynamics of wave packets.

### THEOREM: AN EQUIVALENCE BETWEEN SPECTRAL AREA AND SKIN EFFECT

For generic one-dimensional non-Hermitian systems, the correspondence between the spectral shape and the skin effect has been derived [23, 24], i.e., when the Bloch spectrum is a loop-type (an arc-type), the skin effect appears (disappears).

Generalizing the correspondence to two dimensions, we note two main differences. One difference is in the periodic-boundary spectrum,  $E_i(\mathbf{k})$ , where  $i$  is the band index and  $\mathbf{k}$  the crystal momentum in the first Brillouin zone (BZ). Generally speaking,  $E_i(\mathbf{k})$  is a mapping from the  $d$ -dimensional torus to the complex plane,  $\mathbb{C}$ . When  $d = 1$ , the image of  $E_i(k)$  forms a loop; but when  $d > 1$ , the image is generically a continuum on  $\mathbb{C}$ , denoted by  $E_i(\text{BZ})$ . The area covered by  $E_i(\text{BZ})$  on the complex plane is called the *spectral area*, denoted by  $A_i$ . Another difference is in the variety of open-boundary condition. There is only one geometry for an open system in one dimension, i.e., an open chain; but there are an infinite number of geometries in two dimensions such as triangle, rectangle and pentagon.

Now we are ready to state the theorem of universal skin effect: in the thermodynamic limit, the skin effect is present in a hamiltonian having open boundary of arbitrary geometry, if the spectral area is nonzero ( $A_i \neq 0$ ); vice versa, the skin effect is absent for all possible geometries, if the spectral area is zero ( $A_i = 0$ ). As the periodic-boundary hamiltonian describes the dynamics in the bulk, the theorem relates a bulk property (spec-

tral area) to a boundary one (existence of skin modes). Fig. 1 shows some schematic examples. In the Supplemental Material Sec. I, a complete proof of the theorem has been provided.

The above theorem has implied the universality of skin effect in two and higher dimensions. As  $E_i(\text{BZ})$  is the image of the  $d \geq 2$ -dimensional torus on the complex plane, it takes fine tuning of parameters to make  $A_i = 0$  for every  $i$ . In fact, for single-band hamiltonian, we can prove that  $A = 0$  if and only if  $\mathcal{H}(\mathbf{k}) = P[h(\mathbf{k})]$ , where  $h(\mathbf{k})$  is a Hermitian hamiltonian and  $P$  is a polynomial. In other words, a randomly generated non-Hermitian hamiltonian  $\mathcal{H}(\mathbf{k})$  has skin effect: the first meaning of universality. In previous studies, other types of skin effect, such as the line-skin and the high-order-skin effect, in two and higher dimensions have been proposed [42, 48]. These types all require the open-boundary system take a special geometry (usually a rectangle) and are hence considered special and non-generic. The skin effect when  $A_i \neq 0$  assumes a completely generic geometry of boundary: the second meaning of universality. The third meaning of universality lies in the fact that, unlike in one dimension, higher-dimensional skin effect is compatible with all spatial symmetries. A standing wave explanation for the above theorem is provided in the Supplemental Material Sec. II.

### THE CORNER-SKIN AND THE GEOMETRY-DEPENDENT-SKIN EFFECT

While the theorem shows that the skin effect is universal, it does not specify what skin modes look like in higher dimensions. Here, we report two types of the universal skin effect, the corner-skin effect (CSE) and the geometry-dependent skin effect (GDSE). Note that the CSE we mentioned in this paper has the nature of non-

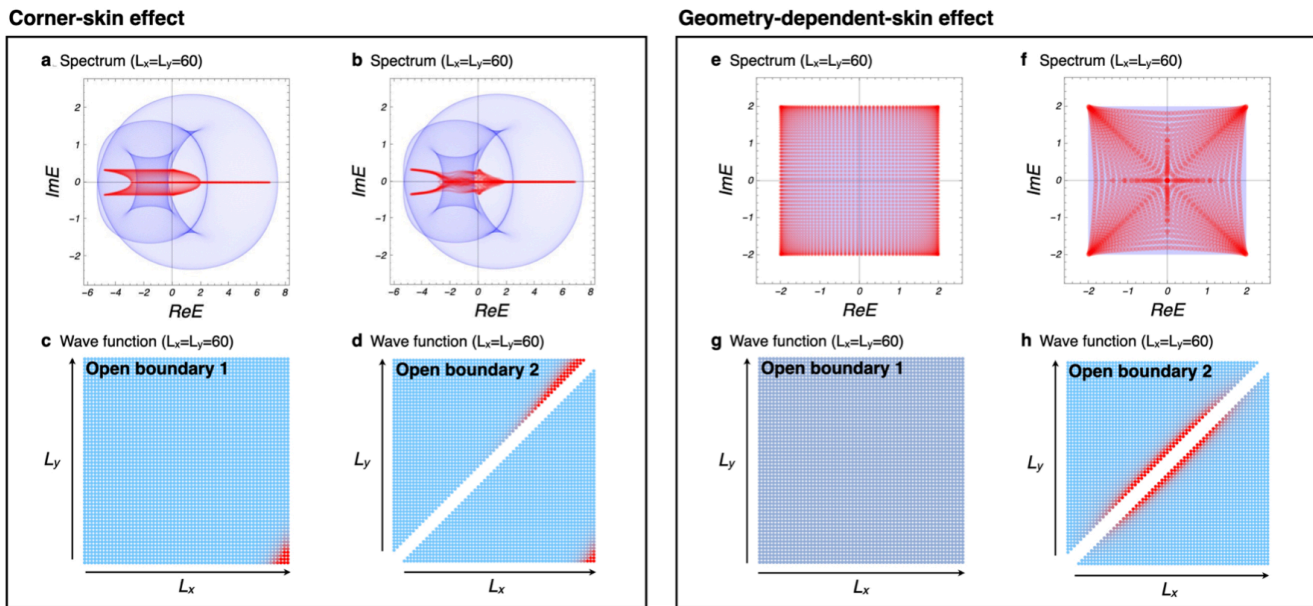


FIG. 2. Two manifestations of skin effect. One is the CSE (a)-(d), the other is the GDSE (e)-(h). In in (a)(b)(e)(f), the light blue regions represent the spectrum under periodic boundary, and the red points represent the eigenvalues under different open-boundary geometries. The spatial distributions of eigenstates  $W(\mathbf{x})$  are plotted in (c)(d)(g)(h). The GDSE disappears under square geometry (open boundary 1) in (g), and reappears under triangle geometry (open boundary 2) in (h).

reciprocity, similar to the one-dimensional skin effect.

The hamiltonian of the example for CSE is

$$\mathcal{H}(\mathbf{k}) = [5(\cos k_x + \cos 2k_x) - i(\sin k_x + 3 \sin 2k_x) + 5 \cos k_y + i \sin k_y]/2, \quad (1)$$

of which the spectral area under square geometry and triangle geometry is shown in Fig. 2 (a)(b) with light blue color. Because of the nonzero spectral area, the theorem tells us that the hamiltonian must have the universal skin effect. This is verified in Fig. 2 (c)(d), where the spatial distributions of all the eigenstates

$$W(\mathbf{x}) = \frac{1}{N} \sum_n |\psi_n(\mathbf{x})|^2 \quad (2)$$

under different open boundaries are plotted. Here  $\psi_n(x)$  is a normalized eigenstate and  $N$  is the number of eigenstates. It is found that the wave functions are always localized at the corner of the boundary in Fig. 2(c), even if the open-boundary geometry is changed in Fig. 2(d). We also plot the corresponding eigenvalue spectra under different open boundaries, as shown in Fig. 2 (a)(b) with red color. One can notice that the spectral areas under periodic and open boundaries do not equal. This kind of skin effect is called CSE, which can be explained by a nonzero current functional

$$J_\alpha[n] = \sum_i \oint_{\text{BZ}} dk^d n(E_i, E_i^*) \partial_{k_\alpha} E_i(\mathbf{k}) \quad (3)$$

under the periodic-boundary condition, where  $n(E, E^*)$  is any smooth function [23]. The current functional

is shown to vanish in two and three dimensions under point groups  $C_i$ ,  $D_{2,3,4,6}$ ,  $C_{2h,3h,4h,6h}$ ,  $D_{2d,3d,2h,3h,4h,6h}$ ,  $T$ ,  $T_d$ ,  $O$  and  $O_h$ . Therefore, the CSE is only compatible with point groups  $C_m$  and  $C_{2,3,4,6,2v,3v,4v,6v}$  (see details in the Supplemental Material Sec. III).

The hamiltonian of the example for GDSE reads

$$\mathcal{H}(\mathbf{k}) = 2 \cos k_x + 2i \cos k_y. \quad (4)$$

Since the spectral area is nonzero, our theorem tells us that the system must have skin effect for generic geometry, such as a random polygon. However, an interesting phenomenon in this example is that the skin effect disappears under the square geometry due to the existence of two mirror symmetries shown in Fig. 2 (g). Once we choose other types of boundaries where mirror symmetries are broken, the skin effect reappears as shown in Fig. 2 (h). Since the emergence of the skin effect and the position of localization depend on the geometry, it is called the GDSE. Besides the distribution of the eigenstates, another feature of the GDSE is that area of the open-boundary spectrum seems to be the same as  $A_i$ . However, the corresponding density of states is dependent by the choice of geometry as shown in Fig. 2 (e)(f). We conjecture this is a universal phenomenon for the GDSE. In the Supplemental Material Sec. III, we have provided some additional examples to illustrate this new type of skin effect, and shown that the increase in the number of skin modes is proportional to the increase in the system volume. For GDSE, there is at least one spatial geometry such that skin modes vanish, and as such is mutually exclusive with CSE. Additionally, GDSE is compatible with all point groups, in contrast to CSE.

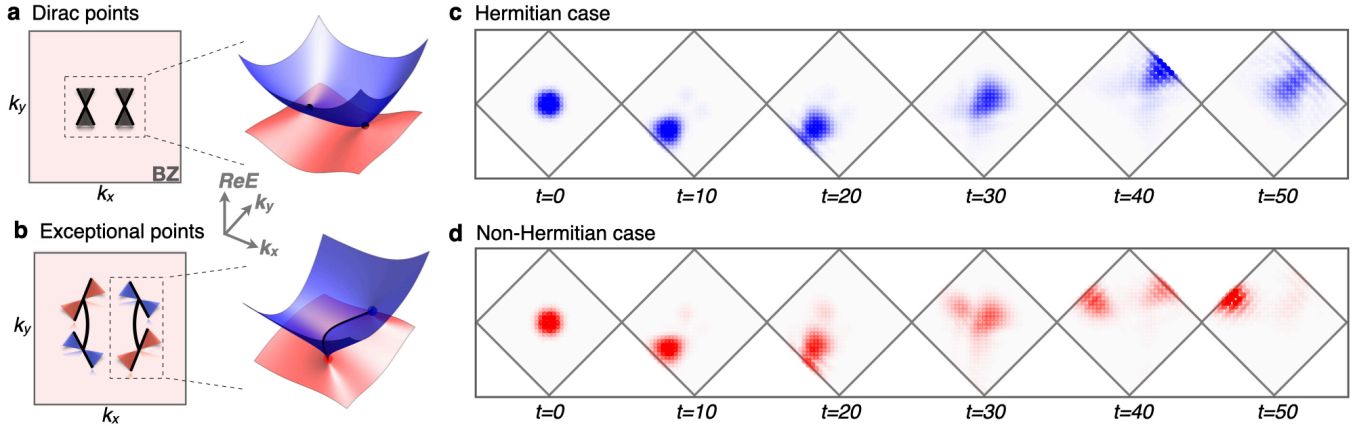


FIG. 3. Two Dirac points (a) of a two-dimensional photonic crystal model are split into four exceptional points (b) upon adding non-Hermitian term, such as radiational loss. Correspondingly, the evolution of Gaussian wave packet with initial velocity at the center of a diamond geometry for each ten time intervals is shown in (c) with  $\gamma = 0$  (Hermitian) and (d) with  $\gamma = 1/4$  (GDSE).

### COROLLARY: SKIN EFFECT FROM EXCEPTIONAL POINTS

An immediate corollary of our theorem is that all lattice hamiltonians having stable exceptional points have universal skin effect, connecting two unique phenomena in the non-Hermitian band theory. Consider a stable branch point  $\mathbf{k}_0$  in two dimensions. Due to the branch point structure of exceptional point, the dispersion around  $\mathbf{k}_0$  can be expressed as  $E_{\pm}(\mathbf{k}) = \pm c_0 \sqrt{q_x + c_1 q_y} + O(|\mathbf{k} - \mathbf{k}_0|)$ , where  $q_{i=x,y}$  denotes a small derivation from exceptional point in  $x$  or  $y$  direction, that is,  $q_i = k_i - k_{0i}$ . Here  $c_0, c_1$  are nonzero complex numbers and  $c_1 \notin \mathbb{R}$ . Suppose the range of the expansion is  $r_0$ , then it is clear that  $A_{\pm} \geq |c_0| \pi r_0^2 / 2 \neq 0$ . By the theorem, the system must have skin effect (see more details in the Supplementary Material Sec. IV).

Now we use the photonic crystal model that has been experimentally realized in Ref. [73] to demonstrate our corollary. The tight-binding model hamiltonian with periodic boundary can be written as

$$H(\mathbf{k}) = \mathbf{d}(\mathbf{k}) \cdot \boldsymbol{\sigma} - i\gamma/2(\sigma_0 - \sigma_z), \quad (5)$$

where  $\boldsymbol{\sigma} = (\sigma_0, \sigma_x, \sigma_y, \sigma_z)$  is a vector of the Pauli matrices and  $\mathbf{d}(\mathbf{k})$  is a vector with four components, that is,

$$\mathbf{d}(\mathbf{k}) = \{ \mu_0 - (t_2 + t_3)(\cos k_x + \cos k_y), \\ t_1[1 - \cos k_x - \cos k_y + \cos(k_x - k_y)], \\ t_1[\sin k_x - \sin k_y - \sin(k_x - k_y)], \\ \mu_z + (t_2 - t_3)(\cos k_x - \cos k_y) \}. \quad (6)$$

The parameters are chosen as follows,  $(t_1, t_2, t_3, \mu_0, \mu_z) = (0.4, -0.1, 0.5, 1.35, -0.02)$ . As shown in Fig. 3 (a), in the Hermitian limit, i.e.  $\gamma = 0$ , the system has two Dirac points along the  $x$ -axis. When external dissipation or radiational loss is added, i.e.,  $\gamma \neq 0$ , each Dirac

point splits into two exceptional points shown in Fig. 2 (b), connected by the bulk Fermi arc. According to our theorem, the system must have the universal skin effect, more precisely, the GDSE shown in the Supplementary Material Sec. IV. The skin effect disappears under square geometry but reappears under diamond geometry shown in Fig. 3 (c)(d). In this case, the majority of the eigenstates are concentrated on the four edges.

As mentioned in the previous discussion, the appearance of the skin effect can be reflected in the dynamical properties. In order to show this, we simulate the time evolution of the wave packets with initial velocity at the center of the diamond geometry. Here the initial state is chosen to be Gaussian form  $|\psi_0\rangle = \mathcal{N} \exp[-(x - x_0)^2/10 - (y - y_0)^2/10 - i2x - i2y](1, 1)^T$ , where  $\mathcal{N}$  is the normalization factor and  $x_0 = y_0 = 21$  is the center coordinate of the diamond geometry. We plot the corresponding normalized final states  $|\psi(t_f)\rangle = \mathcal{N}(t_f) e^{-i\mathcal{H}_{\text{OBC}} t_f} |\psi_0\rangle$  for every ten time intervals, where  $\mathcal{H}_{\text{OBC}}$  represents the open-boundary hamiltonian on the diamond geometry. As shown in Fig. 3 (c), in the Hermitian case, the center of the wave packets obeys the reflection rule. Since the initial velocity of the wave packet is perpendicular to the two edges, the center of the wave packet just bounces between the two edges regardless of the dispersion of the wave packet. However, in the non-Hermitian case ( $\gamma = 1/4$ ) with GDSE, besides the normal reflection channel, the wave packet will evolve into the upper left boundary as shown in Fig. 3 (d). This anomalous dynamical behavior is a experimental signature of GDSE.

We also propose the realization for CSE in a three-dimensional system with exceptional lines in the Supplementary Material Sec. IV. Experimentally, the non-reciprocity of the CSE can be detected by two-point Green function approach.

## DISCUSSION

Our work has built a bridge between two distinct phenomena that only exist in non-Hermitian systems, i.e., the exceptional points (lines) and the non-Hermitian skin effect, by establishing the correspondence between bulk (spectral area) and boundary (universal skin effect). We prove that the skin effect be universal and compatible with all spatial symmetries and reciprocity in two and higher dimensions. Due to the universality, it is expected that the skin effect is observable in a wide range of platforms, such as photonic crystals with natural radiational loss, acoustic metamaterials and circuit networks with lossy components such as resistors. Beyond these classical systems, the skin effect can also be realized in con-

densed matter, e.g., the heavy-fermion material with finite quasiparticle lifetime and the Weyl-exceptional-ring semimetal. The latter is realizable in Weyl semimetals made from inverting bands that have disparate effective masses, such as d- and f-bands.

One should be reminded, however, that the results in this paper assume the coherent dynamics of the constituent degrees of freedom, which is unlikely the case in macroscopic condensed-matter systems where the coherence length is shorter than the system size. On the contrary, for the systems where the system size and the coherent length are comparable, as in mesoscopic systems, we believe that the universal skin effect has a significant contribution to the transport properties, a subject for future exploration.

- 
- [1] G. Gamow, “Zur Quantentheorie des Atomkernes,” *Zeitschrift für Physik* **51**, 204–212 (1928).
- [2] Liang Feng, Ramy El-Ganainy, and Li Ge, “Non-Hermitian photonics based on parity–time symmetry,” *Nature Photonics* **11**, 752–762 (2017).
- [3] Ramy El-Ganainy, Konstantinos G. Makris, Mercedes Khajavikhan, Ziad H. Musslimani, Stefan Rotter, and Demetrios N. Christodoulides, “Non-Hermitian physics and PT symmetry,” *Nature Physics* **14**, 11–19 (2018).
- [4] Tomoki Ozawa, Hannah M. Price, Alberto Amo, Nathan Goldman, Mohammad Hafezi, Ling Lu, Mikael C. Rechtsman, David Schuster, Jonathan Simon, Oded Zeitler, and Iacopo Carusotto, “Topological photonics,” *Rev. Mod. Phys.* **91**, 015006 (2019).
- [5] Vladyslav Kozii and Liang Fu, “Non-Hermitian Topological Theory of Finite-Lifetime Quasiparticles: Prediction of Bulk Fermi Arc Due to Exceptional Point,” arXiv:1708.05841 (2017).
- [6] Huitao Shen and Liang Fu, “Quantum Oscillation from In-Gap States and a Non-Hermitian Landau Level Problem,” *Phys. Rev. Lett.* **121**, 026403 (2018).
- [7] Michał Papaj, Hiroki Isobe, and Liang Fu, “Nodal arc of disordered Dirac fermions and non-Hermitian band theory,” *Phys. Rev. B* **99**, 201107 (2019).
- [8] Yuki Nagai, Yang Qi, Hiroki Isobe, Vladyslav Kozii, and Liang Fu, “DMFT Reveals the Non-Hermitian Topology and Fermi Arcs in Heavy-Fermion Systems,” *Phys. Rev. Lett.* **125**, 227204 (2020).
- [9] Daniel Leykam, Konstantin Y. Bliokh, Chunli Huang, Y. D. Chong, and Franco Nori, “Edge Modes, Degeneracies, and Topological Numbers in Non-Hermitian Systems,” *Phys. Rev. Lett.* **118**, 040401 (2017).
- [10] Yong Xu, Sheng-Tao Wang, and L.-M. Duan, “Weyl Exceptional Rings in a Three-Dimensional Dissipative Cold Atomic Gas,” *Phys. Rev. Lett.* **118**, 045701 (2017).
- [11] Huitao Shen, Bo Zhen, and Liang Fu, “Topological Band Theory for Non-Hermitian Hamiltonians,” *Phys. Rev. Lett.* **120**, 146402 (2018).
- [12] Emil J. Bergholtz, Jan Carl Budich, and Flore K. Kunst, “Exceptional topology of non-Hermitian systems,” *Rev. Mod. Phys.* **93**, 015005 (2021).
- [13] Zongping Gong, Yuto Ashida, Kohei Kawabata, Kazuaki Takasan, Sho Higashikawa, and Masahito Ueda, “Topological Phases of Non-Hermitian Systems,” *Phys. Rev. X* **8**, 031079 (2018).
- [14] Jong Yeon Lee, Junyeong Ahn, Hengyun Zhou, and Ashvin Vishwanath, “Topological Correspondence between Hermitian and Non-Hermitian Systems: Anomalous Dynamics,” *Phys. Rev. Lett.* **123**, 206404 (2019).
- [15] Yuto Ashida, Zongping Gong, and Masahito Ueda, “Non-Hermitian Physics,” arXiv:2006.01837 (2020).
- [16] Kohei Kawabata, Ken Shiozaki, Masahito Ueda, and Masatoshi Sato, “Symmetry and Topology in Non-Hermitian Physics,” *Phys. Rev. X* **9**, 041015 (2019).
- [17] Shunyu Yao and Zhong Wang, “Edge States and Topological Invariants of Non-Hermitian Systems,” *Phys. Rev. Lett.* **121**, 086803 (2018).
- [18] Shunyu Yao, Fei Song, and Zhong Wang, “Non-Hermitian Chern Bands,” *Phys. Rev. Lett.* **121**, 136802 (2018).
- [19] Flore K. Kunst, Elisabet Edvardsson, Jan Carl Budich, and Emil J. Bergholtz, “Biorthogonal Bulk-Boundary Correspondence in Non-Hermitian Systems,” *Phys. Rev. Lett.* **121**, 026808 (2018).
- [20] V. M. Martinez Alvarez, J. E. Barrios Vargas, and L. E. F. Foa Torres, “Non-Hermitian robust edge states in one dimension: Anomalous localization and eigenspace condensation at exceptional points,” *Phys. Rev. B* **97**, 121401(R) (2018).
- [21] Ching Hua Lee and Ronny Thomale, “Anatomy of skin modes and topology in non-Hermitian systems,” *Phys. Rev. B* **99**, 201103(R) (2019).
- [22] Kazuki Yokomizo and Shuichi Murakami, “Non-Bloch Band Theory of Non-Hermitian Systems,” *Phys. Rev. Lett.* **123**, 066404 (2019).
- [23] Kai Zhang, Zhesen Yang, and Chen Fang, “Correspondence between Winding Numbers and Skin Modes in Non-Hermitian Systems,” *Phys. Rev. Lett.* **125**, 126402 (2020).
- [24] Nobuyuki Okuma, Kohei Kawabata, Ken Shiozaki, and Masatoshi Sato, “Topological Origin of Non-Hermitian Skin Effects,” *Phys. Rev. Lett.* **124**, 086801 (2020).
- [25] Zhesen Yang, Kai Zhang, Chen Fang, and Jiangping Hu, “Non-Hermitian Bulk-Boundary Correspondence and Auxiliary Generalized Brillouin Zone Theory,” *Phys. Rev. Lett.* **125**, 226402 (2020).
- [26] Yifei Yi and Zhesen Yang, “Non-Hermitian Skin Modes

- Induced by On-Site Dissipations and Chiral Tunneling Effect,” *Phys. Rev. Lett.* **125**, 186802 (2020).
- [27] Linhu Li, Ching Hua Lee, and Jiangbin Gong, “Topological Switch for Non-Hermitian Skin Effect in Cold-Atom Systems with Loss,” *Phys. Rev. Lett.* **124**, 250402 (2020).
- [28] Dan S. Borgnia, Alex Jura Kruchkov, and Robert-Jan Slager, “Non-Hermitian Boundary Modes and Topology,” *Phys. Rev. Lett.* **124**, 056802 (2020).
- [29] Stefano Longhi, “Probing non-Hermitian skin effect and non-Bloch phase transitions,” *Phys. Rev. Research* **1**, 023013 (2019).
- [30] S. Longhi, “Non-Bloch-Band Collapse and Chiral Zener Tunneling,” *Phys. Rev. Lett.* **124**, 066602 (2020).
- [31] Linhu Li, Ching Hua Lee, Sen Mu, and Jiangbin Gong, “Critical non-Hermitian skin effect,” *Nature Communications* **11**, 5491 (2020).
- [32] Ye Xiong, “Why does bulk boundary correspondence fail in some non-hermitian topological models,” *Journal of Physics Communications* **2**, 035043 (2018).
- [33] Zhesen Yang, “Non-perturbative Breakdown of Bloch’s Theorem and Hermitian Skin Effects,” arXiv:2012.03333 (2020).
- [34] N. W. Ashcroft and N. D. Mermin, *Solid State Physics* (Holt-Saunders, 1976).
- [35] Lei Xiao, Tianshu Deng, Kunkun Wang, Gaoyan Zhu, Zhong Wang, Wei Yi, and Peng Xue, “Non-Hermitian bulk–boundary correspondence in quantum dynamics,” *Nature Physics* **16**, 761–766 (2020).
- [36] Lei Xiao, Tianshu Deng, Kunkun Wang, Zhong Wang, Wei Yi, and Peng Xue, “Observation of non-Bloch parity-time symmetry and exceptional points,” (2020), arXiv:2009.07288.
- [37] T. Helbig, T. Hofmann, S. Imhof, M. Abdelghany, T. Kiessling, L. W. Molenkamp, C. H. Lee, A. Szameit, M. Greiter, and R. Thomale, “Generalized bulk–boundary correspondence in non-Hermitian topoelectrical circuits,” *Nature Physics* **16**, 747–750 (2020).
- [38] Sebastian Weidemann, Mark Kremer, Tobias Helbig, Tobias Hofmann, Alexander Stegmaier, Martin Greiter, Ronny Thomale, and Alexander Szameit, “Topological funneling of light,” *Science* **368**, 311–314 (2020).
- [39] Martin Brandenbourger, Xander Locsin, Edan Lerner, and Corentin Coulais, “Non-reciprocal robotic metamaterials,” *Nature Communications* **10**, 4608 (2019).
- [40] Ananya Ghatak, Martin Brandenbourger, Jasper van Wezel, and Corentin Coulais, “Observation of non-hermitian topology and its bulk–edge correspondence in an active mechanical metamaterial,” *Proceedings of the National Academy of Sciences* **117**, 29561–29568 (2020).
- [41] Kai Wang, Avik Dutt, Ki Youl Yang, Casey C. Wojcik, Jelena Vučković, and Shanhui Fan, “Generating arbitrary topological windings of a non-Hermitian band,” *Science* **371**, 1240–1245 (2021).
- [42] Ching Hua Lee, Linhu Li, and Jiangbin Gong, “Hybrid Higher-Order Skin-Topological Modes in Nonreciprocal Systems,” *Phys. Rev. Lett.* **123**, 016805 (2019).
- [43] Motohiko Ezawa, “Non-Hermitian boundary and interface states in nonreciprocal higher-order topological metals and electrical circuits,” *Phys. Rev. B* **99**, 121411 (2019).
- [44] Motohiko Ezawa, “Non-Hermitian higher-order topological states in nonreciprocal and reciprocal systems with their electric-circuit realization,” *Phys. Rev. B* **99**, 201411 (2019).
- [45] Tobias Hofmann, Tobias Helbig, Frank Schindler, Nora Salgo, Marta Brzezińska, Martin Greiter, Tobias Kiessling, David Wolf, Achim Vollhardt, Anton Kabaši, Ching Hua Lee, Ante Bilušić, Ronny Thomale, and Titus Neupert, “Reciprocal skin effect and its realization in a topoelectrical circuit,” *Phys. Rev. Research* **2**, 023265 (2020).
- [46] Tao Liu, Yu-Ran Zhang, Qing Ai, Zongping Gong, Kohei Kawabata, Masahito Ueda, and Franco Nori, “Second-Order Topological Phases in Non-Hermitian Systems,” *Phys. Rev. Lett.* **122**, 076801 (2019).
- [47] Tsuneya Yoshida, Tomonari Mizoguchi, and Yasuhiro Hatsugai, “Mirror skin effect and its electric circuit simulation,” *Phys. Rev. Research* **2**, 022062(R) (2020).
- [48] Kohei Kawabata, Masatoshi Sato, and Ken Shiozaki, “Higher-order non-Hermitian skin effect,” *Phys. Rev. B* **102**, 205118 (2020).
- [49] Colin Scheibner, William T. M. Irvine, and Vincenzo Vitelli, “Non-Hermitian Band Topology and Skin Modes in Active Elastic Media,” *Phys. Rev. Lett.* **125**, 118001 (2020).
- [50] Zhiwang Zhang, María Rosendo López, Ying Cheng, Xiaojun Liu, and Johan Christensen, “Non-Hermitian Sonic Second-Order Topological Insulator,” *Phys. Rev. Lett.* **122**, 195501 (2019).
- [51] Xi-Wang Luo and Chuanwei Zhang, “Higher-Order Topological Corner States Induced by Gain and Loss,” *Phys. Rev. Lett.* **123**, 073601 (2019).
- [52] Elisabet Edvardsson, Flore K. Kunst, and Emil J. Bergholtz, “Non-Hermitian extensions of higher-order topological phases and their biorthogonal bulk–boundary correspondence,” *Phys. Rev. B* **99**, 081302 (2019).
- [53] Yuhao Ma and Taylor L. Hughes, “The Quantum Skin Hall Effect,” (2020), arXiv:2008.02284.
- [54] Ryo Okugawa, Ryo Takahashi, and Kazuki Yokomizo, “Second-order topological non-Hermitian skin effects,” *Phys. Rev. B* **102**, 241202 (2020).
- [55] Lucas S. Palacios, Serguei Tchoumakov, Maria Guix, Ignacio Pagonabarraga, Samuel Sánchez, and Adolfo G. Grushin, “Guided accumulation of active particles by topological design of a second-order skin effect,” (2020), arXiv:2012.14496.
- [56] Yiling Song, Weiwei Liu, Lingzhi Zheng, Yicong Zhang, Bing Wang, and Peixiang Lu, “Two-dimensional non-Hermitian Skin Effect in a Synthetic Photonic Lattice,” *Phys. Rev. Applied* **14**, 064076 (2020).
- [57] Yongxu Fu, Jihan Hu, and Shaolong Wan, “Non-hermitian second-order skin and topological modes,” *Phys. Rev. B* **103**, 045420 (2021).
- [58] Yang Yu, Minwoo Jung, and Gennady Shvets, “Zero-energy corner states in a non-Hermitian quadrupole insulator,” *Phys. Rev. B* **103**, L041102 (2021).
- [59] Fei Song, Hong-Yi Wang, and Zhong Wang, “Non-Bloch PT symmetry breaking: Universal threshold and dimensional surprise,” arXiv:2102.02230 (2021).
- [60] Tosio Kato, *Perturbation theory for linear operators*, Vol. 132 (Springer Science & Business Media, 2013).
- [61] Mohammad-Ali Miri and Andrea Alù, “Exceptional points in optics and photonics,” *Science* **363**, eaar7709 (2019).
- [62] Ş. K. Özdemir, S. Rotter, F. Nori, and L. Yang, “Parity-time symmetry and exceptional points in photonics,” *Nature Materials* **18**, 783–798 (2019).
- [63] Zin Lin, Hamidreza Ramezani, Toni Eichelkraut,

- Tsampikos Kottos, Hui Cao, and Demetrios N. Christodoulides, “Unidirectional Invisibility Induced by  $\mathcal{PT}$ -Symmetric Periodic Structures,” *Phys. Rev. Lett.* **106**, 213901 (2011).
- [64] Tony E. Lee, “Anomalous Edge State in a Non-Hermitian Lattice,” *Phys. Rev. Lett.* **116**, 133903 (2016).
- [65] Rafael A. Molina and José González, “Surface and 3D Quantum Hall Effects from Engineering of Exceptional Points in Nodal-Line Semimetals,” *Phys. Rev. Lett.* **120**, 146601 (2018).
- [66] Johan Carlström and Emil J. Bergholtz, “Exceptional links and twisted fermi ribbons in non-hermitian systems,” *Phys. Rev. A* **98**, 042114 (2018).
- [67] Alexander Cerjan, Meng Xiao, Luqi Yuan, and Shan-hui Fan, “Effects of non-Hermitian perturbations on Weyl Hamiltonians with arbitrary topological charges,” *Phys. Rev. B* **97**, 075128 (2018).
- [68] Kohei Kawabata, Takumi Bessho, and Masatoshi Sato, “Classification of Exceptional Points and Non-Hermitian Topological Semimetals,” *Phys. Rev. Lett.* **123**, 066405 (2019).
- [69] Kristof Moors, Alexander A. Zyuzin, Alexander Yu. Zyuzin, Rakesh P. Tiwari, and Thomas L. Schmidt, “Disorder-driven exceptional lines and Fermi ribbons in tilted nodal-line semimetals,” *Phys. Rev. B* **99**, 041116 (2019).
- [70] Zhesen Yang, A. P. Schnyder, Jiangping Hu, and Ching-Kai Chiu, “Fermion Doubling Theorems in Two-Dimensional Non-Hermitian Systems for Fermi Points and Exceptional Points,” *Phys. Rev. Lett.* **126**, 086401 (2021).
- [71] Haoran Xue, Qiang Wang, Baile Zhang, and Y. D. Chong, “Non-Hermitian Dirac Cones,” *Phys. Rev. Lett.* **124**, 236403 (2020).
- [72] Bo Zhen, Chia Wei Hsu, Yuichi Igarashi, Ling Lu, Ido Kaminer, Adi Pick, Song-Liang Chua, John D. Joannopoulos, and Marin Soljačić, “Spawning rings of exceptional points out of Dirac cones,” *Nature* **525**, 354–358 (2015).
- [73] Hengyun Zhou, Chao Peng, Yoseob Yoon, Chia Wei Hsu, Keith A. Nelson, Liang Fu, John D. Joannopoulos, Marin Soljačić, and Bo Zhen, “Observation of bulk Fermi arc and polarization half charge from paired exceptional points,” *Science* **359**, 1009–1012 (2018).
- [74] Xufeng Zhang, Kun Ding, Xianjing Zhou, Jing Xu, and Dafei Jin, “Experimental Observation of an Exceptional Surface in Synthetic Dimensions with Magnon Polaritons,” *Phys. Rev. Lett.* **123**, 237202 (2019).
- [75] Alexander Cerjan, Sheng Huang, Mohan Wang, Kevin P. Chen, Yidong Chong, and Mikael C. Rechtsman, “Experimental realization of a Weyl exceptional ring,” *Nature Photonics* **13**, 623–628 (2019).
- [76] Zhesen Yang and Jiangping Hu, “Non-Hermitian Hopf-link exceptional line semimetals,” *Phys. Rev. B* **99**, 081102 (2019).
- [77] Weiyuan Tang, Xue Jiang, Kun Ding, Yi-Xin Xiao, Zhao-Qing Zhang, C. T. Chan, and Guancong Ma, “Exceptional nexus with a hybrid topological invariant,” *Science* **370**, 1077–1080 (2020).
- [78] M. Michael Denner, Anastasiia Skurativska, Frank Schindler, Mark H. Fischer, Ronny Thomale, Tomáš Bzdušek, and Titus Neupert, “Exceptional Topological Insulators,” (2020), [arXiv:2008.01090](https://arxiv.org/abs/2008.01090).
- [79] Zhesen Yang, Ching-Kai Chiu, Chen Fang, and Jiangping Hu, “Jones Polynomial and Knot Transitions in Hermitian and non-Hermitian Topological Semimetals,” *Phys. Rev. Lett.* **124**, 186402 (2020).
- [80] C. Dembowski, H.-D. Gräf, H. L. Harney, A. Heine, W. D. Heiss, H. Rehfeld, and A. Richter, “Experimental Observation of the Topological Structure of Exceptional Points,” *Phys. Rev. Lett.* **86**, 787–790 (2001).
- [81] C. Dembowski, B. Dietz, H.-D. Gräf, H. L. Harney, A. Heine, W. D. Heiss, and A. Richter, “Observation of a Chiral State in a Microwave Cavity,” *Phys. Rev. Lett.* **90**, 034101 (2003).
- [82] Alois Regensburger, Christoph Bersch, Mohammad-Ali Miri, Georgy Onishchukov, Demetrios N. Christodoulides, and Ulf Peschel, “Parity–time synthetic photonic lattices,” *Nature* **488**, 167–171 (2012).
- [83] Liang Feng, Ye-Long Xu, William S. Fegadolli, Ming-Hui Lu, José E. B. Oliveira, Vilson R. Almeida, Yan-Feng Chen, and Axel Scherer, “Experimental demonstration of a unidirectional reflectionless parity-time metamaterial at optical frequencies,” *Nature Materials* **12**, 108–113 (2013).
- [84] Jan Wiersig, “Enhancing the Sensitivity of Frequency and Energy Splitting Detection by Using Exceptional Points: Application to Microcavity Sensors for Single-Particle Detection,” *Phys. Rev. Lett.* **112**, 203901 (2014).
- [85] T. Gao, E. Estrecho, K. Y. Bliokh, T. C. H. Liew, M. D. Fraser, S. Brodbeck, M. Kamp, C. Schneider, S. Höfling, Y. Yamamoto, F. Nori, Y. S. Kivshar, A. G. Truscott, R. G. Dall, and E. A. Ostrovskaya, “Observation of non-Hermitian degeneracies in a chaotic exciton-polariton billiard,” *Nature* **526**, 554–558 (2015).
- [86] H. Xu, D. Mason, Luyao Jiang, and J. G. E. Harris, “Topological energy transfer in an optomechanical system with exceptional points,” *Nature* **537**, 80–83 (2016).
- [87] Jörg Doppler, Alexei A. Mailybaev, Julian Böhm, Ulrich Kuhl, Adrian Girschik, Florian Libisch, Thomas J. Milburn, Peter Rabl, Nimrod Moiseyev, and Stefan Rotter, “Dynamically encircling an exceptional point for asymmetric mode switching,” *Nature* **537**, 76–79 (2016).
- [88] Zhong-Peng Liu, Jing Zhang, Şahin Kaya Özdemir, Bo Peng, Hui Jing, Xin-You Lü, Chun-Wen Li, Lan Yang, Franco Nori, and Yu-xi Liu, “Metrology with  $\mathcal{PT}$ -Symmetric Cavities: Enhanced Sensitivity near the  $\mathcal{PT}$ -Phase Transition,” *Phys. Rev. Lett.* **117**, 110802 (2016).
- [89] Hossein Hodaei, Absar U. Hassan, Steffen Wittek, Hipolito Garcia-Gracia, Ramy El-Ganainy, Demetrios N. Christodoulides, and Mercedeh Khajavikhan, “Enhanced sensitivity at higher-order exceptional points,” *Nature* **548**, 187–191 (2017).
- [90] Weijian Chen, Şahin Kaya Özdemir, Guangming Zhao, Jan Wiersig, and Lan Yang, “Exceptional points enhance sensing in an optical microcavity,” *Nature* **548**, 192–196 (2017).
- [91] Jae Woong Yoon, Youngsun Choi, Choloong Hahn, Gunpyo Kim, Seok Ho Song, Ki-Yeon Yang, Jeong Yub Lee, Yongsung Kim, Chang Seung Lee, Jai Kwang Shin, Hong-Seok Lee, and Pierre Berini, “Time-asymmetric loop around an exceptional point over the full optical communications band,” *Nature* **562**, 86–90 (2018).
- [92] M. Z. Hasan and C. L. Kane, “Colloquium: Topological insulators,” *Rev. Mod. Phys.* **82**, 3045–3067 (2010).
- [93] N. P. Armitage, E. J. Mele, and Ashvin Vishwanath, “Weyl and Dirac semimetals in three-dimensional solids,” *Rev. Mod. Phys.* **90**, 015001 (2018).





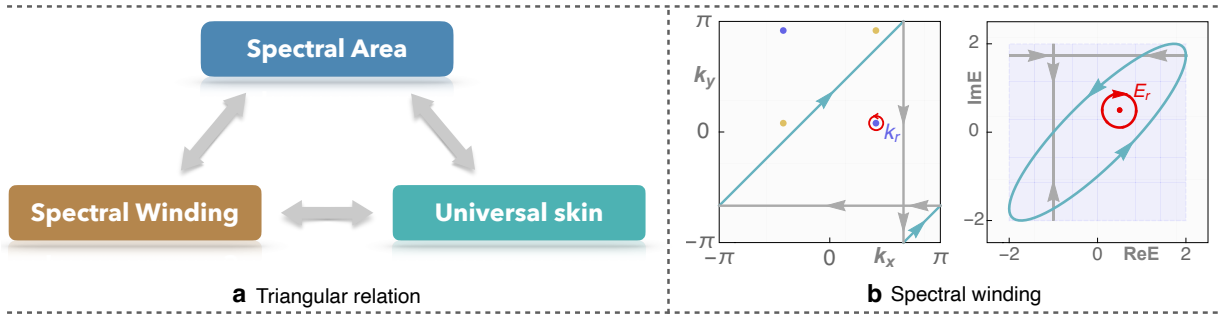


FIG. S2. (a) shows the equivalence relation between spectral area, spectral winding and the universal skin effect. Each equivalence relation is sufficient and necessary. (b) illustrates the spectral winding for hamiltonian Eq. S13. Here the light blue region represents the periodic boundary spectrum, and the paths on BZ corresponds to the spectral loops (or arcs) on the complex plane with the same color.

the localization behaviors, namely, the emergence of skin effect, as shown in Fig. S1 (c-d). In order to illustrate the localization properties,

$$W(x) = \frac{1}{N} \sum_n |\psi_n(x)|^2 \quad (\text{S2})$$

is plotted in Fig. S1 (c-d), where  $\psi_n(x)$  is the  $n$ -th normalized eigenstate of the open boundary hamiltonian, and  $N$  is the number of open boundary eigenstates. For the second example, since the spectral area is zero, as shown in Fig. S1 (f), there is no skin effect. Indeed,  $W(x)$  shown in Fig. S1 (g-h) are extended.

In the following subsection, we will prove the theorem in two-dimensional systems. Our strategy of the proof is illustrated in Fig. S2(a). The equivalence relation between “spectral area” and “the universal skin effect” is linked by “spectral winding” (see the following discussion).

## B. The proof of the theorem in two-dimensions

### 1. Spectral area and spectral winding

We begin with a two-dimensional single-band non-Hermitian model with periodic boundary in both  $x$  and  $y$  directions

$$\mathcal{H}(\mathbf{k}) = u(\mathbf{k}) + iv(\mathbf{k}), \quad (\text{S3})$$

where  $u$  and  $v$  are real functions about  $\mathbf{k} = (k_x, k_y)$ . For any  $\mathbf{k}_r \in \text{BZ}$ , one can define the following winding number

$$\nu(\mathbf{k}_r) = \oint_{\Gamma_{\mathbf{k}_r}} \frac{d\mathbf{k}}{2\pi i} \cdot \nabla_{\mathbf{k}} \log \det[\mathcal{H}(\mathbf{k}) - E_r], \quad \mathbf{k}_r \in \text{BZ}, \quad (\text{S4})$$

where  $\Gamma_{\mathbf{k}_r}$  represents the infinitesimal counterclockwise loop enclosing  $\mathbf{k}_r$ . Here  $E_r = \mathcal{H}(\mathbf{k}_r)$  represents the reference energy, which is shown in Fig. S2 (b) with red point. We note that for different  $\mathbf{k}_r$ , the reference energy is different. This topological invariant describes the spectral winding on the complex plane. As shown in Fig. S2 (b), if  $\nu(\mathbf{k}_r)$  is nonzero, the image of  $\Gamma_{\mathbf{k}_r}$ , i.e.  $\mathcal{H}(\Gamma_{\mathbf{k}_r})$ , forms a closed loop that encloses  $E_r$ .

First we prove the following two statements,

1. if there are some  $\mathbf{k}_r$  points in the BZ with nonzero topological charge, the spectral area must be nonzero;
2. if all the  $\mathbf{k}_r$  points on the BZ have zero topological charge, the spectral area must be zero.

The above two statement can be represented by the equivalence relation between “spectral winding” and “spectral area” shown in Fig. S2 (a).

Based on the definition of winding number, the statement 1 is obvious. Therefore, we only need to prove the statement 2. In order to show this, we expand the hamiltonian at the point  $\mathbf{k}_r \equiv (k_x^r, k_y^r)$  as follows

$$\mathcal{H}(\mathbf{k}) - \mathcal{H}(\mathbf{k}_r) \approx \partial_x \mathcal{H}(\mathbf{k}_r) q_x + \partial_y \mathcal{H}(\mathbf{k}_r) q_y, \quad (\text{S5})$$

where  $q_x, q_y$  are the displacements  $\mathbf{k} - \mathbf{k}_r$  in  $x, y$  directions respectively. For a generic  $\mathbf{k}_r$  point, the first derivative of  $\mathcal{H}$  does not vanish, i.e., the coefficients of  $q_x$  and  $q_y$  in Eq. (S5) cannot be zero at the same time. The reason is that in order to make  $\partial_x \mathcal{H}(\mathbf{k}_r) = \partial_y \mathcal{H}(\mathbf{k}_r) = 0$ , four independent real conditions,  $\text{Re}[\partial_x \mathcal{H}(\mathbf{k}_r)] = \text{Im}[\partial_x \mathcal{H}(\mathbf{k}_r)] = \text{Re}[\partial_y \mathcal{H}(\mathbf{k}_r)] = \text{Im}[\partial_y \mathcal{H}(\mathbf{k}_r)] = 0$ , need to be satisfied. However, in two dimensions, there are only two free parameters  $(k_x, k_y)$ , which cannot satisfy the above four equations generally.

In order to calculate the topological charge of a generic  $\mathbf{k}_r$  point, according to Eq. (S3), one can define

$$C(\mathbf{k}_r) = \begin{pmatrix} \partial_x u(\mathbf{k}_r) & \partial_y u(\mathbf{k}_r) \\ \partial_x v(\mathbf{k}_r) & \partial_y v(\mathbf{k}_r) \end{pmatrix}, \quad (\text{S6})$$

where the notation  $\partial_{x/y}$  refers to  $\partial/\partial k_{x/y}$ . When  $\det[C(\mathbf{k}_r)] \neq 0$ , the topological charge of  $\mathbf{k}_r$  is the sign of the determinant of  $C(\mathbf{k}_r)$ , expressed as

$$\nu(\mathbf{k}_r) = \text{sgn}[\det[C(\mathbf{k}_r)]]. \quad (\text{S7})$$

Therefore, a sufficient and necessary condition for the zero charge for each  $\mathbf{k} \in \text{BZ}$  is

$$\det[C(\mathbf{k})] = \partial_x u(\mathbf{k})\partial_y v(\mathbf{k}) - \partial_y u(\mathbf{k})\partial_x v(\mathbf{k}) = 0. \quad (\text{S8})$$

A theorem (the corollary of theorem 13.2) in Ref. [1] tells us that if  $C(\mathbf{k}) \neq 0$  and  $\det[C(\mathbf{k})] = 0$ , for an open set  $S$ , then,  $u(\mathbf{k})$  and  $v(\mathbf{k})$  have a functional dependent relation with  $\mathbf{k} \in S \subset \text{BZ}$ . Applying the theorem to the entire BZ (except for some isolated points at which the first derivative vanishes), one can reexpress the single-band hamiltonian that satisfies Eq. (S8) as

$$\mathcal{H}(\mathbf{k}) = P[h(\mathbf{k})], \quad (\text{S9})$$

where  $h(\mathbf{k})$  is a real and periodic function of  $\mathbf{k}$ , and  $P$  is a complex polynomial of  $h$ . Since  $h(\mathbf{k})$  is a real periodic function, its image must be an arc on the real axis, e.g.  $h(\mathbf{k}) \in [h_1, h_2]$ , where  $h_{1/2}$  are real numbers. Therefore, the image of  $P[h(\mathbf{k})]$  is also an arc on the complex plane. This completes the proof of the statement 2 for single-band models.

Generalizing the above discussion to the multi-band case, for each  $\mathbf{k}_r \in \text{BZ}$ , the topological charge defined for the  $m$ -th band is

$$\begin{aligned} \nu_m(\mathbf{k}_r) &= \oint_{\Gamma_{\mathbf{k}_r}} \frac{d\mathbf{k}}{2\pi i} \cdot \nabla_{\mathbf{k}} \log \det[\mathcal{H}(\mathbf{k}) - E_m(\mathbf{k}_r)] \\ &= \sum_n \oint_{\Gamma_{\mathbf{k}_r}} \frac{d\mathbf{k}}{2\pi i} \cdot \nabla_{\mathbf{k}} \log[E_n(\mathbf{k}) - E_m(\mathbf{k}_r)], \end{aligned} \quad (\text{S10})$$

where  $E_m(\mathbf{k}_r)$  is the energy of the  $m$ -th band with the momentum  $\mathbf{k}_r$ . For the second equal sign in Eq. (S10), we have used  $\det[\mathcal{H}(\mathbf{k}) - E_m(\mathbf{k}_r)] = \prod_n [E_n(\mathbf{k}) - E_m(\mathbf{k}_r)]$ . For Eq. (S10), if  $\mathbf{k}_r$  is not the degeneracy point, only  $n = m$  term in the summation has contributions to the topological charge. Therefore, the Eq. (S10) further becomes

$$\nu_m(\mathbf{k}_r) = \oint_{\Gamma_{\mathbf{k}_r}} \frac{d\mathbf{k}}{2\pi i} \cdot \nabla_{\mathbf{k}} \log[E_m(\mathbf{k}) - E_m(\mathbf{k}_r)]. \quad (\text{S11})$$

Using the similar approaches in the single-band case, one can conclude that, the the real and imaginary parts of  $E_m(\mathbf{k})$  are locally functional dependent on the neighbourhood of  $\mathbf{k} \in \text{BZ}$ . As a result, the spectrum of  $E_m(\mathbf{k})$  must be an arc. The above conclusion applies for each band. So far, we have proved that if each  $\mathbf{k}$  point on the BZ has zero topological charge, the spectral area must be zero.

## 2. Spectral winding and the universal skin effect

In the above contents, we have proved the equivalence relation between ‘‘spectral winding’’ and ‘‘spectral area’’. Here, we will prove the equivalence condition between ‘‘spectral winding’’ and ‘‘universal skin effect’’, as shown in Fig. S2 (a).

We first notice that the BZ in two-dimensional systems can be covered by a set of straight lines of any slope, labeled as  $\{L_s\}$ . Here, the subscript  $s$  indicates the slope of the set  $\{L_s\}$ , and  $L_s$  represents a generic straight line belonging to  $\{L_s\}$ . For example, if we fix  $k_y(k_x)$  and change  $k_x(k_y)$  from 0 to  $2\pi$ , we get a horizontal (vertical) straight line

with the slope being 0 ( $\infty$ ) on BZ, and the set of all horizontal or vertical straight lines ( $\{L_0\}$  or  $\{L_\infty\}$ ) covers the entire BZ. Particularly, an inclined straight line goes out from one side of BZ and again enters from another side as shown in Fig. S2(b). Since the straight lines on the BZ are periodic, one can define the spectral winding number for each straight lines with respect to the prescribed reference energy  $E_r$ .

$$\nu(L_s, E_r) = \oint_{L_s} \frac{d\mathbf{k}}{2\pi i} \cdot \nabla_{\mathbf{k}} \log \det[\mathcal{H}(\mathbf{k}) - E_r]. \quad (\text{S12})$$

Obviously, if all the  $\mathbf{k}$  points on the BZ have zero topological charge,  $\nu(L_s, E_r)$  must be zero for arbitrary  $L_s$  and  $E_r$ . Otherwise, one can always find some  $L_s$ , such that  $\nu(L_s, E_r)$  is nonzero. Next we briefly prove the latter statement. Assuming that each straight line in  $\{L_0\}$  and  $\{L_\infty\}$  has zero spectral winding, and there is a  $\mathbf{k}_r$  point carrying nonzero topological charge on the BZ. For a generic inclined straight line, one can always find corresponding horizontal and vertical straight lines, such that together with the inclined straight line to form a closed path enclosing  $\mathbf{k}_r$  on BZ. Therefore, the closed path has nonzero winding number with respect to  $E_r$ . Due to the zero spectral winding of the horizontal and vertical straight lines as we assumed, hence a generic inclined straight line must have nonzero spectral winding number.

Let's use an example to show this. Consider the following hamiltonian

$$\mathcal{H}(k_x, k_y) = 2 \cos k_x + 2i \sin k_y. \quad (\text{S13})$$

As shown in Fig. S2, the spectrum of the hamiltonian along each horizontal or vertical straight line (gray lines) on BZ has zero winding number with respect to any reference energy on the spectral area (lightblue square region). However, once we choose the straight line with darker cyan color, these three straight lines (two gray lines with the darker cyan line) together form a closed path that encloses  $\mathbf{k}_r$ . Therefore, the closed path has nonzero spectral winding number with respect to  $E_r$ . Due to the zero spectral winding of two gray lines, the darker cyan straight line must have nonzero winding number for  $E_r$  as illustrated in Fig. S2(b).

If the system has no skin effect under a specific parallelepiped open boundary, the winding number  $\nu_m(L_m, E_r)$  along each straight lines that are perpendicular to the boundary cut directions should be zero. (This is a conjecture that we cannot exactly proved currently. However, we believe this statement is true as all the numerical results we obtained obey this conclusion. Furthermore, it is also a natural generalization of the one-dimensional results [2, 3] and has been mentioned or applied in some recent works [4, 5]) More generally, if the system has no skin effect under any parallelepiped open boundary, then the spectral windings of all straight lines on BZ are required to be zero, which is satisfied when the spectral area of the system is zero. Therefore, nonzero spectral area means that there must be skin effect under certain open boundaries, namely, the existence of the universal skin effect.

### C. The proof of the theorem in three-dimensions

In this section, we extend the above proof of two-dimensional systems into three dimensions. We obtain the similar conclusion that nonzero spectral area is equivalent to the existence of the universal skin effect.

Consider a general three-dimensional single-band tight-binding hamiltonian, which consists of real- and imaginary-part functions

$$\mathcal{H}(k_x, k_y, k_z) = u(k_x, k_y, k_z) + iv(k_x, k_y, k_z). \quad (\text{S14})$$

We choose a generic  $\mathbf{k}_r$  point and use its energy  $\mathcal{H}(\mathbf{k}_r)$  as the reference energy. For a given reference energy  $E_r$ , we can obtain a one-dimensional curve in the there-dimensional BZ by solving the following two real equations,

$$\begin{aligned} u(k_x, k_y, k_z) &= \text{Re}(E_r); \\ v(k_x, k_y, k_z) &= \text{Im}(E_r). \end{aligned} \quad (\text{S15})$$

Each equation determines a surface, and the intersection of two surfaces is one-dimensional curve in there-dimensional BZ. The tangent direction of the curve at  $\mathbf{k}_r$  is perpendicular to the normal vector of the two surfaces at this  $\mathbf{k}_r$  point. The tangent vector at  $\mathbf{k}_r$  is expressed as

$$\mathbf{T}_{\mathbf{k}_r} = \nabla u(\mathbf{k}_r) \times \nabla v(\mathbf{k}_r), \quad (\text{S16})$$

where  $\nabla u(\mathbf{k}_r)$  represents the gradient of  $u$ . We choose the local coordinate system ( $R^3$  space) with  $\mathbf{k}_r$  as the origin, and the gradient is reexpressed as

$$\nabla u(\mathbf{k}_r) = \partial_x u(\mathbf{k}_r) q_x + \partial_y u(\mathbf{k}_r) q_y + \partial_z u(\mathbf{k}_r) q_z, \quad (\text{S17})$$

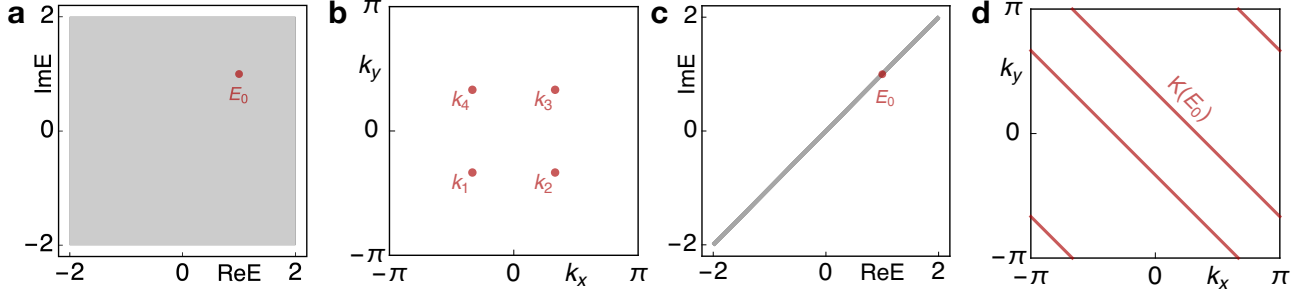


FIG. S3. (a) shows the periodic-boundary spectrum of Eq. (S25) with gray color, and the pre-images of  $E_0 = 1 + i$  (red point in (a)) are the four red points in (b). The periodic-boundary spectrum of Eq. (S26) is the gray line in (c), and  $\mathbf{k}(E_0 = 1 + i)$  is plotted by the red lines in (d).

where  $q_i \equiv \left(\frac{\mathbf{k} - \mathbf{k}_0}{|\mathbf{k} - \mathbf{k}_0|}\right)_i$ ,  $\mathbf{k}$  and  $\mathbf{k}_0$  represent two vectors in the global coordinate system.

Next we expand the hamiltonian into Taylor series around the origin of the local coordinate system,

$$\mathcal{H}(\mathbf{k}) - \mathcal{H}(\mathbf{k}_r) = \sum_{i=x,y,z} \partial_i \mathcal{H}(\mathbf{k}_r) q_i + o(|\mathbf{q}|), \quad (\text{S18})$$

where the subscription  $i$  represents the partial differential to  $x, y, z$ . And  $q_i$  represents the deviation of  $k_i$  from  $k_{r,i}$  and the last term is the infinitesimal of higher order of  $|\mathbf{q}|$ . Obvious, the zero winding condition requires

$$\begin{aligned} \partial_x u(\mathbf{k}_r) \partial_y v(\mathbf{k}_r) - \partial_x v(\mathbf{k}_r) \partial_y u(\mathbf{k}_r) &= 0; \\ \partial_x v(\mathbf{k}_r) \partial_z u(\mathbf{k}_r) - \partial_x u(\mathbf{k}_r) \partial_z v(\mathbf{k}_r) &= 0; \\ \partial_y u(\mathbf{k}_r) \partial_z v(\mathbf{k}_r) - \partial_y v(\mathbf{k}_r) \partial_z u(\mathbf{k}_r) &= 0, \end{aligned} \quad (\text{S19})$$

or equivalently,

$$\mathbf{T}_{\mathbf{k}_r} = \mathbf{0}. \quad (\text{S20})$$

Next, we prove that if all  $\mathbf{k}$  points in three-dimensional BZ satisfy  $\mathbf{T}_{\mathbf{k}} = \mathbf{0}$ , then the entire 3D periodic-boundary spectrum must be an arc in the complex plane. We define a two-tuple function  $W(\mathbf{k}) := [u(\mathbf{k}) \ v(\mathbf{k})]^t$  with three variables, the exterior derivative of the vector-valued function is expressed as

$$dW = \begin{pmatrix} \partial_x u(\mathbf{k}) & \partial_y u(\mathbf{k}) & \partial_z u(\mathbf{k}) \\ \partial_x v(\mathbf{k}) & \partial_y v(\mathbf{k}) & \partial_z v(\mathbf{k}) \end{pmatrix}. \quad (\text{S21})$$

Eq. (S20) implies that the rank of  $dW$  less than 2 (the number of components of  $W$ ). To be precise, there are the following cases. (i.) Both the gradients of  $u$  and  $v$  are not zero vector, and they are linearly dependent on each other. (ii.) One of the gradients of  $u$  and  $v$  is zero vector. (iii.) Both the gradients of  $u$  and  $v$  are zero vector. In all these cases, we can obtain the final conclusion that  $u$  and  $v$  are linearly functional dependent on each other. Therefore, the spectrum must be arcs on the complex plane.

A 3D BZ can be divided into a series of plane systems, each plane corresponds to a two-dimensional subsystem. If the spectral area of a three-dimensional system is nonzero, then for each reference energy on the spectral area, its preimage (1D ring) has nonzero topological charge. Equivalently, the two-dimensional subsystem, of which the BZ (2D plane) has intersections with the ring, also has nonzero topological charge for the intersecting  $k$  points. Hence, the 2D subsystem has nonzero spectral area, and has the universal skin effect. Correspondingly, we come to the same conclusion in 3D systems that nonzero spectral area signifies the existence of the universal skin effect.

## II. A PHYSICAL EXPLANATION FOR THE THEOREM

Here, we use some examples to illustrate the intuition that motivates the theorem. Consider the following one-dimensional model

$$\mathcal{H}_0(k) = 2 \cos k \quad (\text{S22})$$

placed on a chain of length  $L$ . Under the periodic boundary condition, the two Bloch waves  $e^{ik_0x}$  and  $e^{-ik_0x}$  have the same energy  $E(k_0) = 2 \cos k_0$ . When the system has open boundary condition, the Bloch wave  $e^{ik_0x}$  will be reflected to  $e^{-ik_0x}$  with a  $\pi$ -phase shift. Their linear superposition  $e^{ik_0x} - e^{-ik_0x}$  is an eigenstate with energy  $2 \cos k_0$  that satisfies the zero boundary condition at  $x = 0, L$ , thus being an open-boundary eigenstate. When the system is added a momentum-dependent dissipation,

$$\mathcal{H}(k) = 2 \cos k + i \sin k, \quad (\text{S23})$$

the spectrum  $E(k)$  becomes complex and forms an ellipse in the complex plane. In this case, the degeneracy is broken, e.g.  $E(k) \neq E(-k)$ , which implies the open-boundary eigenstates are no longer the linear superposition of the extended Bloch waves. This implies the emergence of skin effect.

Extend the above arguments to two dimensions, and we can provide a physical explanation for the theorem proved in the section I.

Formally, we consider a single-band model

$$\mathcal{H}(\mathbf{k}) = \mathcal{H}_0(\mathbf{k}) + i\Gamma(\mathbf{k}). \quad (\text{S24})$$

When the real and imaginary parts of which are functionally independent, the hamiltonian will have a non-zero spectral area. For a given eigenvalue  $E_0$  of the Bloch hamiltonian, by solving  $\mathcal{H}_0(\mathbf{k}) = \text{Re } E_0$  and  $\Gamma(\mathbf{k}) = \text{Im } E_0$ , one can obtain a finite set of pre-images of  $E_0$ , i.e.  $\mathbf{K}(E_0) = \{\mathbf{k}_1, \dots, \mathbf{k}_m\}$ , which includes all Bloch waves having energy  $E_0$ . Now suppose that one of the Bloch waves  $\mathbf{k}_i \in \mathbf{K}(E_0)$  is incident on the boundary, depending on the normal direction of the boundary, the corresponding momentum of the reflected wave can be arbitrary. However, the number of elements of  $\mathbf{K}(E_0)$  is finite, and as such cannot support so many reflection channels. This failure of reflection mechanism at a generic boundary means the failure in forming an open boundary eigenstate from Bloch waves, which implies the emergence of skin effect under a generic open-boundary geometry. However, the spectrum collapses into an arc (zero spectral area) if the real and imaginary parts of the hamiltonian are functionally dependent, and the number of the corresponding solutions of  $\mathcal{H}(\mathbf{k}) = E_0$  is infinite. It means that there are infinite reflection channels to satisfy the open boundary of any shape, and an open boundary eigenstate can be formed from superimposing all Bloch-wave channels.

Concretely, we choose two examples to demonstrate the above arguments. The first example is

$$\mathcal{H}(\mathbf{k}) = 2 \cos k_x + 2i \cos k_y, \quad (\text{S25})$$

of which the spectral area is nonzero shown in Fig. S3(a). For a given eigenvalue  $E_0 = 1 + i$ , by solving  $2 \cos k_x = 1$  and  $2 \cos k_y = 1$ , we can obtain a finite set of pre-images of  $E_0$ , that is,  $\mathbf{K}(E_0) = \{k_1, k_2, k_3, k_4\}$  [red points in Fig. S3(b)]. The finite solutions of  $\mathcal{H}(\mathbf{k}) = E_0$  cannot support so many reflection channels, that is to say, cannot form an open-boundary eigenstate on a generic geometry by superimposing these Bloch waves specified by  $k_{i=1,2,3,4}$ . Therefore, the hamiltonian Eq. (S25) has skin effect under open-boundary geometry of a generic shape. The second example reads

$$\mathcal{H}(\mathbf{k}) = 2 \cos (k_x + k_y) + 2i \cos (k_x + k_y), \quad (\text{S26})$$

the periodic-boundary spectrum of which is an arc [the gray line in Fig. S3(c)]. The set of pre-images of  $E_0 = 1 + i$  has infinite elements [the red lines in Fig. S3(d)], which means that there are infinite ways of superimposing these Bloch waves to satisfy the open boundary condition of any shape. Therefore, the hamiltonian Eq. (S26) has no skin effect under any open-boundary geometry.

### III. CORNER-SKIN EFFECT AND GEOMETRY-DEPENDENT-SKIN EFFECT

In this section, we will provide some examples to demonstrate the characteristics of the two manifestations of the universal skin effect. We discuss the role of symmetry on the universal skin effect. We define the current functional to explain the appearance of corner-skin effect. In addition, we numerically verified that geometry-dependent-skin effect obeys the volume law, which is a significant feature to distinguish skin modes from conventional boundary states.

#### A. Symmetry and the universal skin effect

We have proved that if the system has nonzero spectral area, the universal skin effect will occur under a general open boundary condition. According to the symmetry restriction, the universal skin effect has two manifestations,

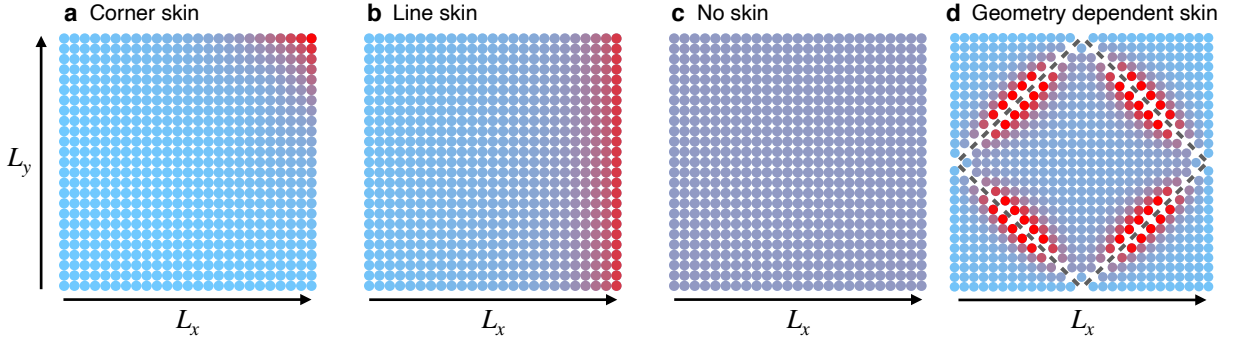


FIG. S4. The distribution of  $W(x)$  for Hamiltonian Eq. (S27) with different parameters and on different geometries. The system size is  $L_x = L_y = 25$ . The probability density is proportional to the opacity of the red color. (a) shows the corner-skin effect with  $t_1 = t_2 = 1, w = 0$ ; (b) shows line skin with  $t_1 = 1, t_2 = w = 0$ ; (c) has no skin effect with  $t_1 = t_2 = 0, w = 1$ , and geometry-dependent-skin effect appears in (d) under triangle and diamond geometries.

that is, corner-skin effect and geometry-dependent-skin effect. Consider a system with nonzero spectral area, if its Hamiltonian has no any symmetry, the skin modes are localized at one or several vertices on an open geometry of any shape, and the number of modes are proportional to the volume of the system. If the Hamiltonian has certain spatial symmetries, such as mirror symmetry, the corner-skin effect will be forbidden. The reason is that the corner-skin effect has the nature of non-reciprocity, which is incompatible with mirror symmetry. However, if we change the open boundary geometry such that the symmetry is broken on the boundary, then geometry-dependent-skin modes will appear, which is a unique but universal phenomenon in higher-dimensional systems. We take a concrete example to demonstrate the role of symmetry on the skin effect. Consider a tight-binding model, of which the periodic-boundary Hamiltonian reads

$$H(k_x, k_y) = h_0(k_x, k_y) + ih_1(k_x, k_y) \\ = \sin k_x \sigma_x + \sin k_y \sigma_y + (2 - \cos k_x - \cos k_y) \sigma_z + i[t_1 \sin k_x + t_2 \sin k_y + w(\cos k_x - \cos k_y)] \sigma_z, \quad (\text{S27})$$

where  $h_0$  and  $h_1$  are the Hermitian and non-Hermitian parts, respectively. The Hermitian part is in a gapless phase with a Dirac point at  $k_x = k_y = 0$ , and has inversion symmetry  $\sigma_z h_0(k_x, k_y) \sigma_z = h_0(-k_x, -k_y)$ .

If we only add the  $w$  non-Hermitian term ( $t_1 = t_2 = 0; w = 1$ ), the combined mirror and non-Hermitian time-reversal symmetry  $M_x T = A_t$  and  $M_y T = \sigma_z A_t$  are preserved ( $A_t$  representing transpose operator),

$$(M_x T) H(k_x, k_y) (M_x T)^{-1} = H(k_x, -k_y); \\ (M_y T) H(k_x, k_y) (M_y T)^{-1} = H(-k_x, k_y). \quad (\text{S28})$$

There is no skin effect under open boundary with square geometry as shown in Fig. S4(c). However, if we cut the square lattice into triangles and diamond lattices, the skin effect will retrieve on the boundaries that destroy the two symmetries, which is shown in Fig. S4(d).

If we only turn on  $t_1$  non-Hermitian term ( $t_1 = 1; t_2 = w = 0$ ), the Hamiltonian preserves  $M_x T$  symmetry but destroys  $M_y T$  symmetry. In this case, the system has skin modes along  $x$  direction as shown in Fig. S4(b), the number of the skin modes are proportional to the volume of the system. If we add  $t_1$  and  $t_2$  non-Hermitian terms ( $t_1 = t_2 = 1; w = 0$ ), the Hamiltonian destroys the two symmetries, and skin modes will be concentrated on the corner as shown in Fig. S4(a).

## B. Current functional

In this section, we first simply introduce the concept of current functional, then discuss the restrictions of point groups in two and three dimensions on the current functional, a quantity faithfully depicting the appearance of corner-skin effect, which demonstrates that corner-skin effect is only compatible with point groups  $C_m$  and  $C_{2,3,4,6,2v,3v,4v,6v}$ .

1. An introduction to the current functional

We define the current functional to depict the corner-skin effect in  $d$  dimensions.

$$J_\alpha[n] = \sum_i J_{i,\alpha}[n] = \sum_i \oint_{\text{BZ}} dk^d n(E_i, E_i^*) \partial_{k_\alpha} E_i(\mathbf{k}), \quad (\text{S29})$$

where  $i$  is band index, and  $k_\alpha$  is a vector, expressed as  $k_\alpha = \sum_i k_i \mathbf{e}_i$  in  $d$ -dimensional momentum space with unit vector basis  $\mathbf{e}_i$ . Here  $n(E, E^*)$  is a distribution function depending on  $E$  and  $E^*$ , but does not depend on  $k$  explicitly, such as the Bose distribution  $n(E, E^*) = (e^{\text{Re } E(k)/k_B T} - 1)^{-1}$ . If there exists a  $n(E, E^*)$  such that the current functional is nonzero for any  $\alpha$ , then the system must have the corner-skin effect. If for any possible  $n(E, E^*)$  and  $\alpha$ , the current functional is zero, then the system has no corner-skin effect.

For example, we take a single-band tight-binding model [Eq. (1) in the main text] as

$$\mathcal{H}(\mathbf{k}) = [5(\cos k_x + \cos 2k_x) - i(\sin k_x + 3 \sin 2k_x) + 5 \cos k_y + i \sin k_y]/2, \quad (\text{S30})$$

and  $n(E, E^*)$  as  $\text{Im}[\mathcal{H}(\mathbf{k})]$ . In this case,  $J_x$  is equal to  $25\pi^2/2$  and  $J_y$  is equal to  $-5\pi^2/2$ . Hence, the system has corner-skin effect. Another example of tight-binding model [Eq. (3) in the main text] reads

$$\mathcal{H}(\mathbf{k}) = 2 \cos k_x + 2i \cos k_y, \quad (\text{S31})$$

of which the current functional  $J_x = J_y = 0$  regardless of the choose of  $n(E, E^*)$ . Therefore, the hamiltonian has no corner-skin effect (although hosts the geometry-dependent-skin effect due to the existence of two mirror symmetries). Meanwhile, the example also reminds us that certain symmetries may prohibit the corner-skin effect. Next, we will systematically analyze the interplay of point-group symmetries and the corner-skin effect.

2. Corner-skin effect under point groups

Here we consider the hamiltonian with only spatial symmetries (without any anti-unitary symmetry such as non-Hermitian time-reversal symmetry), and investigate the restrictions of the point-group symmetries on the current functional, and further conclude that corner-skin effect is only compatible with point groups  $C_m$  and  $C_{2,3,4,6,2v,3v,4v,6v}$ .

**Inversion:** Consider a system that only has inversion symmetry  $I$ , and each band satisfies  $E_i(\mathbf{k}) = E_i(I\mathbf{k}) = E_i(-\mathbf{k})$ . The current functional for  $i$ -th band can be expressed as

$$J_{i,\alpha}[n] = \oint_{\text{BZ}} dk^d n(E_i, E_i^*) \partial_{k_\alpha} E_i(\mathbf{k}), \quad (\text{S32})$$

which is invariant by replacing  $\mathbf{k}$  with  $\mathbf{k}' \equiv -\mathbf{k}$ . After the transformation, Eq. (S32) becomes

$$\begin{aligned} J_{i,\alpha}[n] &= \oint_{\text{BZ}'} (-1)^d dk'^d n(E_i, E_i^*) \partial_{-k'_\alpha} E_i(-\mathbf{k}') = (-1)^d \oint_{\text{BZ}} (-1)^d dk'^d n(E_i, E_i^*) \partial_{-k'_\alpha} E_i(-\mathbf{k}') \\ &= - \oint_{\text{BZ}} dk'^d n(E_i, E_i^*) \partial_{k'_\alpha} E_i(\mathbf{k}') = - \oint_{\text{BZ}} dk^d n(E_i, E_i^*) \partial_{k_\alpha} E_i(\mathbf{k}) = -J_{i,\alpha}[n] = 0. \end{aligned} \quad (\text{S33})$$

It means that if the hamiltonian has only inversion symmetry, the current functional for each band must be zero regardless of the choose of  $n(E, E^*)$ . Equivalently, the corner-skin effect must vanish in the system with inversion symmetry, and is incompatible with the point groups including inversion symmetry, such as  $C_{i,3i,2h,4h,6h}$ ,  $D_{3d,2h,4h,6h}$ ,  $T_h$  and  $O_h$ .

**Rotation:** Consider a system that is invariant under a point group including rotation operator  $R$ , then  $E_i(\mathbf{k}) = E_i(R\mathbf{k})$ . The Eq. (S32) is also invariant under the transformation from  $\mathbf{k}$  to  $\mathbf{k}' \equiv R^{-1}\mathbf{k} = \sum_{ij} \mathbf{e}_i c_{ij} k_j$ , where  $k_j$  is the  $j$ -th component (along  $\mathbf{e}_j$ ) of  $\mathbf{k}$ . After the transformation, the current functional becomes

$$\begin{aligned} J_{i,\alpha}[n] &= \oint_{\text{BZ}'} \det[J_{\mathbf{k},\mathbf{k}'}] dk'^d n(E_i, E_i^*) \partial_{Rk'_\alpha} E_i(R\mathbf{k}') = \oint_{\text{BZ}} dk'^d n(E, E^*) \partial_{Rk'_\alpha} E_i(\mathbf{k}') \\ &= \oint_{\text{BZ}} dk^d n(E, E^*) \partial_{Rk_\alpha} E_i(\mathbf{k}) = \oint_{\text{BZ}} dk^d n(E, E^*) \partial_{k_\alpha} E_i(\mathbf{k}), \end{aligned} \quad (\text{S34})$$

where  $\det[J_{\mathbf{k},\mathbf{k}'}]$  in the second term is the determinant of the Jacobian  $J_{\mathbf{k},\mathbf{k}'}$  that measures the change of differential volume element under different representations and the sign of  $\det[J_{\mathbf{k},\mathbf{k}'}]$  is positive because the rotational operator

preserves orientation. One can always choose an appropriate basis transformation such that  $\det[J_{\mathbf{k},\mathbf{k}'}] = 1$ . In addition, since the Brillouin zone has the same symmetry group as the hamiltonian and rotational operator  $R$  does not change the orientation, the integral region BZ is invariant under the point group. For example, consider a rotation  $R$  that rotates  $\pi/4$  along  $\mathbf{e}_z$  axis, then  $k_x = -k'_y$  and  $k_y = k'_x$ . The Jacobian matrix can be written as

$$J_{\mathbf{k},\mathbf{k}'} = \begin{pmatrix} \partial_{x'} k_x & \partial_{y'} k_x \\ \partial_{x'} k_y & \partial_{y'} k_y \end{pmatrix} \quad (\text{S35})$$

In this case, the determinant of Jacobian  $\det[J_{\mathbf{k},\mathbf{k}'}]$  is 1.

The last equation of Eq. (S34) requires

$$Rk_\alpha = k_\alpha, \quad (\text{S36})$$

which means that the direction of  $k_\alpha$  is parallel to the rotational axis of  $R$ , equivalently, the component of  $k_\alpha$  perpendicular to the rotational axis must be zero. For example, if  $R$  is a rotation that rotates  $\theta$  along  $\mathbf{e}_z$  axis, that is,

$$R = \begin{pmatrix} \cos \theta & -\sin \theta & 0 \\ \sin \theta & \cos \theta & 0 \\ 0 & 0 & 1 \end{pmatrix}, \quad (\text{S37})$$

then Eq. (S36) restricts  $k_\alpha$  as  $0\mathbf{e}_x + 0\mathbf{e}_y + k_z\mathbf{e}_z$ , along  $\mathbf{e}_z$  axis.

As a consequence, if a point group contains two or more rotations with non-parallel rotational axes, the current functional for each band must be zero. If the point group contains only one rotation, a nonzero current functional for each band is allowed, thus corner-skin effect is compatible with the point groups including only one rotation, such as  $C_{2,3,4,6}$ .

**Mirror:** In a similar way, a mirror symmetry requires

$$Mk_\alpha = k_\alpha \quad (\text{S38})$$

if nonzero current functional for each band is allowed, which means the corner-skin effect is compatible with the group containing only one mirror symmetry, that is,  $C_m$ .

It is notable that an additional rotation symmetry is allowed when the rotational axis lies in the mirror plane, and  $k_\alpha$  is restricted as

$$RMk_\alpha = k_\alpha. \quad (\text{S39})$$

Therefore, the corner-skin effect is also compatible with such point groups, i.e.,  $C_{2v,3v,4v,6v}$ .

In summary, we have explicitly shown that corner-skin effect does not exist under most point groups because the current functional is restricted to zero under such point groups, regardless of the choice of  $n(E, E^*)$ , but is allowed to appear under these point groups, i.e.,

$$\{C_m, C_2, C_3, C_4, C_6, C_{2v}, C_{3v}, C_{4v}, C_{6v}\}. \quad (\text{S40})$$

### C. Volume Law

We numerically show that the geometry-dependent-skin effect satisfies the volume law, that is, the increase in the number of skin modes is proportional to the increase in volume of the system,

$$\delta N_{skin} \propto \delta V. \quad (\text{S41})$$

For example, If the shape of the open boundary is a parallelogram whose side-lengths are  $L_x$  and  $L_y$  as shown in Fig. S5, then,  $V = L_x L_y$ . Our criterion for judging a mode as a skin mode is to check whether ninety percent of the probability density of this mode lies within the boundary we appointed.

Consider a tight-binding model with periodic-boundary Hamiltonian  $\mathcal{H}(k_x, k_y) = 2 \cos k_x + 2i \sin k_y$ , there is no skin effect under square geometry Fig. S5(a), but the skin effect appears under parallelogram geometry Fig. S5(b) due to the spectral area being nonzero, which is geometry-dependent-skin effect. The distributions of  $W(\mathbf{x})$  under different open boundaries are plotted. For parallelogram geometry, we specify the thickness of the boundary to be the width of three unit cells, and use black dashed lines to distinguish the boundary from the bulk. If ninety percent of the probability density of a mode lies in the boundary, we count it as a skin mode. We count the number of skin modes for different volumes ( $\mathcal{L}_x \mathcal{L}_y$ ), and the fitting curve (blue curve in Fig. S5(c)) shows that the two are in a linear relation, that is,  $\delta N_{skin} = 0.52 \delta V$ . The volume law of geometry-dependent-skin effect has been verified numerically.



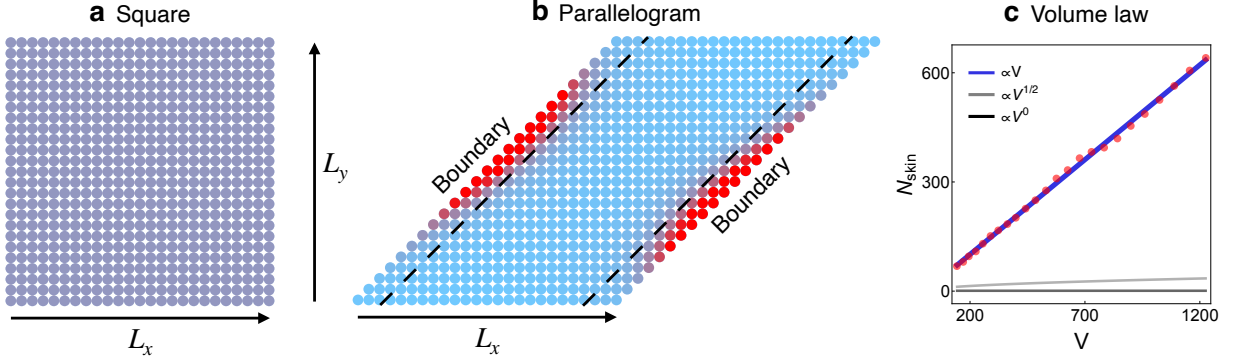


FIG. S5. The norm squared of all wave functions of the Hamiltonian Eq. (S13) on square lattice (a) and parallelogram lattice (b) is plotted. The system size is chosen as  $L_x = L_y = 25$ . The volume law is shown in (c), in which blue line represents  $N_{skin} \propto V$ , gray line  $N_{skin} \propto \sqrt{V}$  and black line  $N_{skin} \propto 1$ .

#### IV. EXCEPTIONAL SEMIMETALS

In this section, we will prove the corollary of our theorem, that is all stable exceptional semimetals imply the universal skin effect. We first review the topological charge of non-Hermitian band degeneracies.

##### A. Non-Hermitian band degeneracy

Consider a general  $m$ -band non-Hermitian Bloch Hamiltonian (with periodic boundary condition),

$$\mathcal{H}(\mathbf{k}) = \sum_{s=1}^{m^2-1} [h_s^r(\mathbf{k}) + ih_s^i(\mathbf{k})] \Gamma_s, \quad (\text{S42})$$

where  $\Gamma_s$  are the generators of Lie algebra  $\mathfrak{su}(m)$  and  $h_s^r(\mathbf{k})$  and  $h_s^i(\mathbf{k})$  are real functions of  $\mathbf{k}$ . When  $m = 2, 3, 4$ ,  $\Gamma_s$  are the Pauli, GellMann, and  $\gamma$  matrices, respectively. The eigenvalues of  $\mathcal{H}(\mathbf{k})$  can be obtained by solving the following characteristic polynomial

$$f_E(\mathbf{k}) = \det[E - \mathcal{H}(\mathbf{k})] = \prod_{i=1}^m [E - E_i(\mathbf{k})], \quad (\text{S43})$$

where  $E_i(\mathbf{k})$  is the  $i$ th eigenvalue of the non-Hermitian Hamiltonian  $\mathcal{H}(\mathbf{k})$ . At the degeneracy point  $\mathbf{k}_D$ , two bands must have the same energy, i.e.

$$E_i(\mathbf{k}_D) = E_j(\mathbf{k}_D) \quad (\text{S44})$$

for some  $i \neq j$ . In Ref. [6, 7], the authors have shown that the above condition is equivalent to the vanishing of the discriminant of  $f_E(\mathbf{k})$ , i.e.

$$\text{Disc}_E[\mathcal{H}](\mathbf{k}_D) = 0, \quad (\text{S45})$$

where

$$\text{Disc}_E[\mathcal{H}](\mathbf{k}) = \prod_{i < j} [E_i(\mathbf{k}) - E_j(\mathbf{k})]^2 \quad (\text{S46})$$

is the discriminant of  $f_E(\mathbf{k})$ . Although the discriminant is defined by the roots of  $f_E(\mathbf{k}) = 0$ , it can be computed directly from the determinant of the Sylvester matrix of  $f_E(\mathbf{k})$  and  $\partial_E f_E(\mathbf{k})$ , which can be expressed by the coefficients of  $f_E(\mathbf{k})$ . Now we show a concrete example of the discriminant method.

**Example:** Consider a generic two-band model

$$\mathcal{H}(\mathbf{k}) = h_0(\mathbf{k})\sigma_0 + h_x(\mathbf{k})\sigma_x + h_y(\mathbf{k})\sigma_y + h_z(\mathbf{k})\sigma_z, \quad (\text{S47})$$

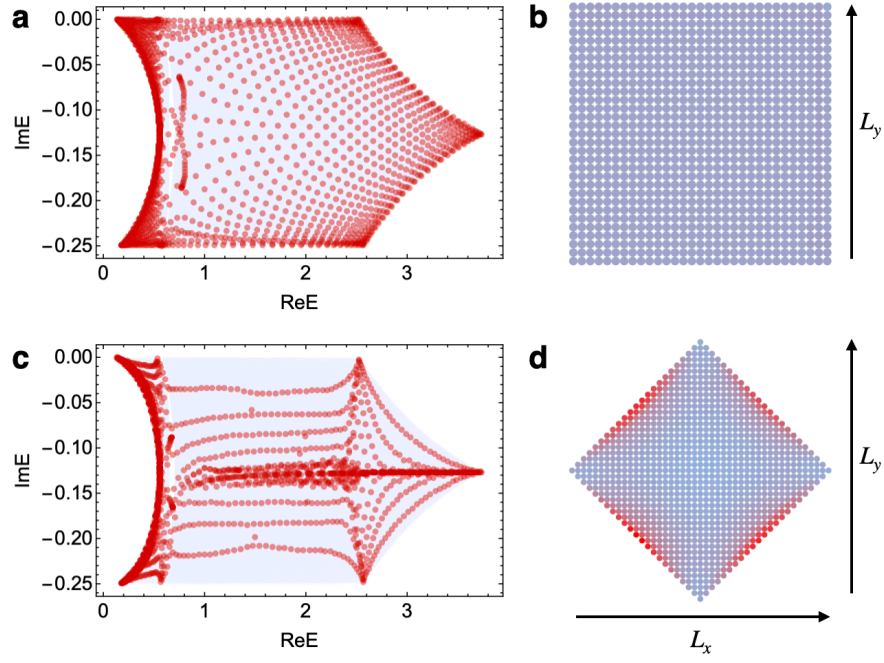


FIG. S6. The periodic-boundary spectrum of the photonic crystal model is shown in (a)(c) with light blue color. Under the square geometry with the systems size  $L_x = L_y = 31$ , the eigenvalues (red points) and the norm squared of all wave functions are shown in (a) and (b), respectively. Under the diamond geometry with the systems size  $L_x = L_y = 45$ , the eigenvalues (red points) and the norm squared of all wave functions are plotted in (c) and (d), respectively.

where  $h_\mu(\mathbf{k}) = h_\mu^r(\mathbf{k}) + ih_\mu^i(\mathbf{k})$  are complex functions of  $\mathbf{k}$ . The characteristic polynomial of the two-band model can be written as

$$f_E(\mathbf{k}) = E^2 + b(\mathbf{k})E + c(\mathbf{k}), \quad (\text{S48})$$

where  $b(\mathbf{k}) = -2h_0(\mathbf{k})$  and  $c(\mathbf{k}) = h_0^2(\mathbf{k}) - h_x^2(\mathbf{k}) - h_y^2(\mathbf{k}) - h_z^2(\mathbf{k})$ . Computing the discriminant of polynomial (S48) with respect to the energy  $E$ , we obtain the following condition for the existence of DPs

$$\text{Disc}_E[\mathcal{H}](\mathbf{k}) = b^2(\mathbf{k}) - 4c(\mathbf{k}) = 4[h_x^2(\mathbf{k}) + h_y^2(\mathbf{k}) + h_z^2(\mathbf{k})] = 0. \quad (\text{S49})$$

This condition can also be obtained from the energy spectrum, that is the two bands  $E_\pm = h_0(\mathbf{k}) \pm ([h_x^2(\mathbf{k}) + h_y^2(\mathbf{k}) + h_z^2(\mathbf{k})]^{1/2})$  are degenerate, whenever the square root is vanishing.

From the above example, one can notice that the discriminant  $\text{Disc}_E[\mathcal{H}](\mathbf{k})$  is a complex periodic function of  $\mathbf{k}$ . Its vanishing is equivalent to the vanishing of the real and imaginary parts, i.e.

$$\text{Re Disc}_E[\mathcal{H}](\mathbf{k}) = \text{Im Disc}_E[\mathcal{H}](\mathbf{k}) = 0. \quad (\text{S50})$$

The solution of the above equation are the non-Hermitian degeneracy points in 2D and lines in 3D.

## B. Topological charge of non-Hermitian band degeneracies

In this subsection, we will review the topological charge of the non-Hermitian band degeneracies. Based on the discriminant of the characteristic polynomial, one can define the topological charge of the degeneracy point  $\mathbf{k}_D$ , i.e.

$$\nu(\mathbf{k}_D) = \frac{1}{2\pi i} \oint_{\Gamma(\mathbf{k}_D)} d\mathbf{k} \cdot \nabla_{\mathbf{k}} \ln \text{Disc}_E[\mathcal{H}](\mathbf{k}). \quad (\text{S51})$$

where  $\Gamma(\mathbf{k}_D)$  is a loop encircling the degeneracy point  $\mathbf{k}_D$ . Since  $\text{Disc}_E[\mathcal{H}](\mathbf{k})$  is single valued, this invariant is quantized, which is called the discriminant number in Ref. [7]. Putting

$$\text{Disc}_E[\mathcal{H}](\mathbf{k}) = \prod_{i < j} [E_i(\mathbf{k}) - E_j(\mathbf{k})]^2 \quad (\text{S52})$$

into  $\nu(\mathbf{k}_D)$ , one can obtain

$$\begin{aligned}
\nu(\mathbf{k}_D) &= \frac{1}{2\pi i} \oint_{\Gamma(\mathbf{k}_D)} d\mathbf{k} \cdot \nabla_{\mathbf{k}} \ln \prod_{1 \leq i < j \leq n} [E_i(\mathbf{k}) - E_j(\mathbf{k})]^2 \\
&= \frac{1}{2\pi i} \sum_{i \neq j} \oint_{\Gamma(\mathbf{k}_D)} d\mathbf{k} \cdot \nabla_{\mathbf{k}} \ln [E_i(\mathbf{k}) - E_j(\mathbf{k})] \\
&= \frac{1}{2\pi} \sum_{i \neq j} \oint_{\Gamma(\mathbf{k}_D)} d\mathbf{k} \cdot \nabla_{\mathbf{k}} \arg [E_i(\mathbf{k}) - E_j(\mathbf{k})].
\end{aligned} \tag{S53}$$

Therefore, for a two-band system,

$$\nu(\mathbf{k}_D) = \frac{1}{2\pi} \oint_{\Gamma(\mathbf{k}_D)} d\mathbf{k} \cdot \nabla_{\mathbf{k}} \arg [E_+(\mathbf{k}) - E_-(\mathbf{k})] \tag{S54}$$

which describes the winding of the complex energy between two bands. Now we show a concrete example of the winding number.

**Example:** Consider the following low energy Hamiltonian around  $\mathbf{k}_D$ ,

$$\mathcal{H}_1(\delta\mathbf{k}) = \sigma_+ + (\delta k_x + i\delta k_y)\sigma_-, \tag{S55}$$

where  $\delta\mathbf{k} = \mathbf{k} - \mathbf{k}_D$  and  $\sigma_{\pm} = (\sigma_x \pm i\sigma_y)/2$ . The eigenvalues of  $\mathcal{H}(\delta\mathbf{k})$  are

$$E_{\pm}(\delta\mathbf{k}) = \pm \sqrt{\delta k_x + i\delta k_y}. \tag{S56}$$

When  $\mathbf{k} = \mathbf{k}_D$ , which is equivalent to  $\delta k_x = \delta k_y = 0$ , one can find  $E_+(\delta\mathbf{k} = 0) = E_-(\delta\mathbf{k} = 0) = 0$ . This means  $\mathbf{k}_D$  is a non-Hermitian degeneracy point. Now we choose  $\Gamma(\mathbf{k}_D) = \mathbf{k}_D + \delta k_r(\cos\theta, \sin\theta)$ , then,

$$E_{\pm}(\delta\mathbf{k}) = \pm \delta k_r^{1/2} e^{i\theta/2}, \quad \theta \in (-\pi, \pi]. \tag{S57}$$

One can find that  $E_+(\delta\mathbf{k})$  and  $E_-(\delta\mathbf{k})$  forms a spectral loop that encloses  $E_+(\mathbf{k}_D) = E_-(\mathbf{k}_D) = 0$ . The winding number  $\nu(\mathbf{k}_D)$  describes this topological properties of degeneracy points.

The topological charge  $\nu(\mathbf{k}_D)$  can be used to classify the non-Hermitian degeneracies. However, the classification is not complete. As a comparison with  $\mathcal{H}_1(\delta\mathbf{k})$ , consider the following two low energy Hamiltonians,

$$\mathcal{H}_2(\delta\mathbf{k}) = (\delta k_x + i\delta k_y)^2 \sigma_+ + (\delta k_x - i\delta k_y) \sigma_-. \tag{S58}$$

Obvious,  $\delta\mathbf{k} = 0$  is a degeneracy point. One can further prove that its topological charge is +1, which is equal to the charge of  $\delta\mathbf{k} = 0$  in  $\mathcal{H}_1(\delta\mathbf{k})$ . However, these two degeneracy points have different properties. For example

$$\mathcal{H}_1(\delta\mathbf{k} = 0) = \sigma_+, \quad \mathcal{H}_2(\delta\mathbf{k} = 0) = 0. \tag{S59}$$

One can notice that  $\mathcal{H}_1(\delta\mathbf{k} = 0)$  is non-diagonal. This type of non-Hermitian degeneracy points are called exceptional points. In Ref. [7], the authors have shown that only the exceptional points with  $\nu(\mathbf{k}_D) = \pm 1$  are robust in 2D. Any other non-Hermitian band degeneracies are unstable against non-Hermitian perturbations.

Having clarifying the topological charge of non-Hermitian degeneracies, now we can prove the corollary of our theorem. Since in 2D, the topological charge of the stable exceptional points must be  $\pm 1$ , the corresponding spectrum area must be nonzero.

### C. The photonic crystal model

In this subsection, we numerically calculate the spectrum and spatial distribution of the wave function, i.e.  $W(x)$  in Eq. S2, for the photonic crystal model in the main text under different geometries.

It shows that the skin effect disappears under square geometry in Fig. S6(b), and reappears under diamond geometry in Fig. S6(d), which is a characteristic signature of geometry-dependent-skin effect. Here we take the non-Hermitian parameter  $\gamma$  as 1/4. The spectrum under square geometry (red points in Fig. S6(a)) coincides with the spectrum of periodic boundary (light blue region in Fig. S6(a)(c)). We conjecture that the spectrum under diamond geometry (red points in Fig. S6(d)) will also coincide with the periodic-boundary spectrum as the system size increases. However, it clearly shows that the density of states under different geometries is completely different. The dependence of density of states on the choice of boundary geometry is another significant feature of geometry-dependent-skin effect.

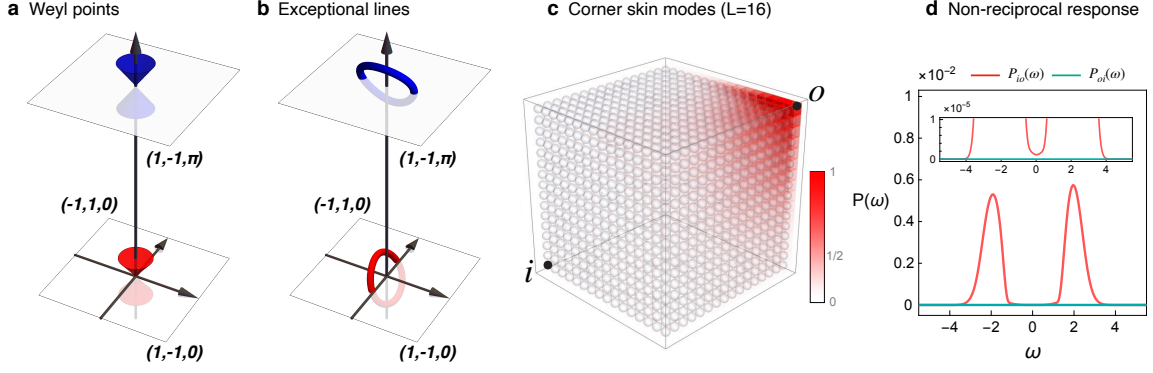


FIG. S7. Two Weyl points (a) of a three-dimensional Weyl semimetal are expanded into two exceptional rings (b) after the addition of non-Hermitian perturbations. The spatial distribution of eigenstate is plotted in (c). The modulus square of the propagator from  $i$  to  $o$   $P_{io}(\omega)$  and that from  $o$  to  $i$   $P_{oi}(\omega)$ , as functions of  $\omega$ , are plotted with red color and dark cyan color in (d), respectively.

#### D. The corner-skin effect in a three-dimensional exceptional-line semimetal

We propose the realization for corner-skin effect in a three-dimensional system with exceptional lines. Consider a Weyl semimetal with non-Hermitian term as a perturbation, of which the periodic-boundary hamiltonian reads

$$H(k) = [\mathbf{d}_r(k) + i\delta\mathbf{d}_i(k)] \cdot \boldsymbol{\sigma}, \quad (\text{S60})$$

where  $\mathbf{d}_r(k)$  and  $\mathbf{d}_i(k)$  are vectors with four components, that is,

$$\begin{aligned} \mathbf{d}_r(k) &= (0, \sin k_x, \sin k_y, 2 - \cos k_x - \cos k_y + \sin k_z), \\ \mathbf{d}_i(k) &= (-\sqrt{5}, 1 + \cos k_z, 1 - \cos k_z, \cos k_z). \end{aligned} \quad (\text{S61})$$

The Hermitian part  $\mathbf{d}_r \cdot \boldsymbol{\sigma}$  is a Weyl semimetal with two Weyl points. One Weyl point with  $+1$  topological charge [red cone in Fig S7 (a)] is at  $(0, 0, 0)$ , and another with  $-1$  topological charge [blue cone in Fig S7 (a)] is at  $(0, 0, \pi)$ . Upon turning on the non-Hermitian term ( $\delta \neq 0$ ), the Weyl points evolve into two exceptional rings as shown in Fig. S7 (b). According to our theorem, the system with exceptional lines must have the universal skin effect. Specially, the system described in Eq. (S60) always has corner-skin effect as shown in Fig. S7 (c) with  $\delta = 1/6$ .

Due to the non-reciprocity of the corner-skin effect, we propose an experimental approach of two-point Green function to detect the corner-skin effect. We give a source at  $i = (1, 1, 1)$  position, and probe it at  $o = (16, 16, 16)$  position in Fig. S7 (c). The modulus square of the propagator from  $i$  to  $o$  is expressed as

$$P_{io}(\omega) = \sum_{\alpha, \beta=1,2} |\langle o, \beta | \frac{1}{\omega - \hat{H}} | i, \alpha \rangle|^2, \quad (\text{S62})$$

where  $\alpha, \beta$  label the orbitals of the unit cell. We calculate  $P_{io}(\omega)$  and plot it with red color in Fig. S7 (d). We do the same process but interchange  $i$  and  $o$ , and  $P_{oi}(\omega)$  is plotted with dark cyan color in Fig. S7 (d). A significant difference between  $P_{io}(\omega)$  and  $P_{oi}(\omega)$  demonstrates the non-reciprocity of corner-skin effect.

- 
- [1] Lynn Harold Loomis and Shlomo Sternberg, *Advanced calculus* (World Scientific, 1968).
  - [2] Kai Zhang, Zhesen Yang, and Chen Fang, ‘‘Correspondence between Winding Numbers and Skin Modes in Non-Hermitian Systems,’’ *Phys. Rev. Lett.* **125**, 126402 (2020).
  - [3] Nobuyuki Okuma, Kohei Kawabata, Ken Shiozaki, and Masatoshi Sato, ‘‘Topological Origin of Non-Hermitian Skin Effects,’’ *Phys. Rev. Lett.* **124**, 086801 (2020).
  - [4] Kazuki Yokomizo and Shuichi Murakami, ‘‘Non-Bloch Band Theory of Non-Hermitian Systems,’’ *Phys. Rev. Lett.* **123**, 066404 (2019).
  - [5] M. Michael Denner, Anastasiia Skurativska, Frank Schindler, Mark H. Fischer, Ronny Thomale, Tomáš Bzdušek, and Titus Neupert, ‘‘Exceptional Topological Insulators,’’ (2020), [arXiv:2008.01090](https://arxiv.org/abs/2008.01090).

- [6] Zhesen Yang, Ching-Kai Chiu, Chen Fang, and Jiangping Hu, “Jones Polynomial and Knot Transitions in Hermitian and non-Hermitian Topological Semimetals,” [Phys. Rev. Lett. \*\*124\*\*, 186402 \(2020\)](#).
- [7] Zhesen Yang, A. P. Schnyder, Jiangping Hu, and Ching-Kai Chiu, “Fermion Doubling Theorems in Two-Dimensional Non-Hermitian Systems for Fermi Points and Exceptional Points,” [Phys. Rev. Lett. \*\*126\*\*, 086401 \(2021\)](#).